Photoemission Spectroscopy Characterization of Halide Perovskites

Solène Béchu, Maryline Ralaiarisoa, Arnaud Etcheberry, Philip Schulz

Photoemission Spectroscopy Characterization of Halide Perovskites

Solène Béchu, Maryline Ralaiarisoa, Arnaud Etcheberry and Philip Schulz**

Dr Solène Béchu Author 1, Dr Arnaud Etcheberry Author 3
Université Paris-Saclay, UVSQ, CNRS, UMR 8180, Institut Lavoisier de Versailles, 78000, Versailles, France
E-Mail: solene.bechu@uvsq.fr

Dr. Maryline Ralaiarisoa Author 2, Dr. Philip Schulz Author 4
CNRS, Institut Photovoltaïque d'Île de France (IPVF), UMR 9006, 18 boulevard Thomas Gobert, 91120, Palaiseau, France
E-Mail: philip.schulz@cnrs.fr

Keywords: Halide Perovskites, Photoemission Spectroscopy, Electronic Properties, Energy Materials Solar Cells

Controlling the surface and interface properties of halide perovskites (HaPs) materials is key to improve performance and stability of HaP-based solar cells. Here, we give an overview on the use of different photoemission spectroscopy (PES) techniques, a primary tool kit to investigate chemical and electronic properties of surfaces and interfaces, in research on HaP compounds. Our focus is on X-ray Photoelectron Spectroscopy (XPS), Hard X-ray Photoemission Spectroscopy (HAXPES), Ultraviolet Photoemission Spectroscopy (UPS) and Inverse Photoemission Spectroscopy (IPES), highlighting the importance of good practices during PES measurements. Starting from the working principles of PES, we discuss critical measurements conditions. In particular, the exposure of HaP surface to vacuum and high energy radiation can cause accelerated ageing, degradation, and also ionic migration in the sample. We then discuss the impact of these changes on the electronic and chemical properties, and elaborate on the specific challenges encountered when performing PES measurements of HaPs. These include the deviation from pristine surface conditions, determination of "soft" band edges and assessment of band bending. We conclude the review by emphasizing good practices for PES

measurements of HaP samples and outline the scope of *operando* type measurements to capture the transient behavior of HaPs in the experiment.

1.Introduction

Halide perovskites (HaPs) define a class of semiconductors with tunable optoelectronic properties uniquely paired with remarkable mechanical properties.[1,2] They have found widespread application in a broad range of optoelectronic devices such as thin-film photovoltaics, light emitting diodes and radiation sensors.[3–5]

In this review, we examine the use of photoemission spectroscopy (also called photoelectron spectroscopy) to analyze the chemical and electronic properties of HaP surfaces and interfaces in HaP-based devices. Particularly, the role of the interface for device functionality in terms of performance limits and stability has been found to be crucial.[6] However, characterization of these interfaces proved to be challenging due to the complex composition of the HaP material itself, which often includes five or more different elemental and molecular components. We will describe the basic applicability of photoemission spectroscopy (PES), give the scope of HaP material parameters accessible by this characterization, and evaluate best practices for reliable data collection.

The implementation of PES, and more specifically, of the more commonly known X-ray photoemission spectroscopy (XPS), allows the determination of the chemical composition of a sample surface. Furthermore, the technique yields information about the chemical environment of the probed species and hence the atomic bonds. Given the complex stoichiometry of HaPs, we will discuss how a careful analysis of these data becomes paramount to investigate the chemical state of the various components under the predicament that the measurement itself, i.e. exposing the surface to high energetic radiation in vacuum, poses a perturbation to the surface.[7] Given the complex stoichiometry of HaPs, we will discuss how a careful analysis of these data becomes paramount to investigate the chemical state of the various components

under the predicament that the measurement itself, i.e. exposing the surface to high energetic radiation in vacuum, poses a perturbation to the surface. This latter aspect is prevalent for HaP samples which typically consist of volatile and reactive components. Indeed, since the earliest PES reports on perovskites solar cells, stability issues, leading to chemical surface modifications, have been encountered, notably due to the generation of defects under energetic radiation in vacuum.[8–10]

In addition to the chemical analysis, PES offers the possibility to experimentally access key electronic properties, which determine the mode of operation of a semiconductor device in question. Here, the classical semiconductor thin film device exhibits multiple metal–semiconductor, insulator-semiconductor, insulator-metal, and/or semiconductor-semiconductor interfaces, all of which require a distinct model framework and approach to characterization. Considering interfaces in HaP-based devices, electronic transport can primarily be attributed to electrons and holes at the conduction and valence band edges, respectively, if transport via defect-levels remains negligible. Hence, determining the position of the Fermi level (E_F) in the band gap and the relative positions of the band edges with respect to E_F and vacuum level (E_{vac}) becomes of primary interest.

PES measurements give direct experimental access to the band offsets at semiconductor interfaces. In consequence, knowledge of the offset between the conduction band edges of two adjacent semiconducting films determines the electron transport across the interface, while the valence band edge offset describes the transport of holes.

Further energetic quantities can be extracted in the context of the PES experiment as shown in **Figure 1**. These are the work function (WF), which is the distance between E_F and E_{vac} and the ionization energy (IE), which is defined as the energy difference between E_{vac} and valence band maximum (E_{VBM}). Equivalently to the latter, one can implicitly determine the electron affinity (EA), which is the quantity measured between vacuum level and conduction band minimum

(E_{CBM}). On a general note, IE and EA can be understood as the minimum energy required to remove a valence electron from the surface, and the minimum energy released by capturing a free electron from vacuum, respectively.

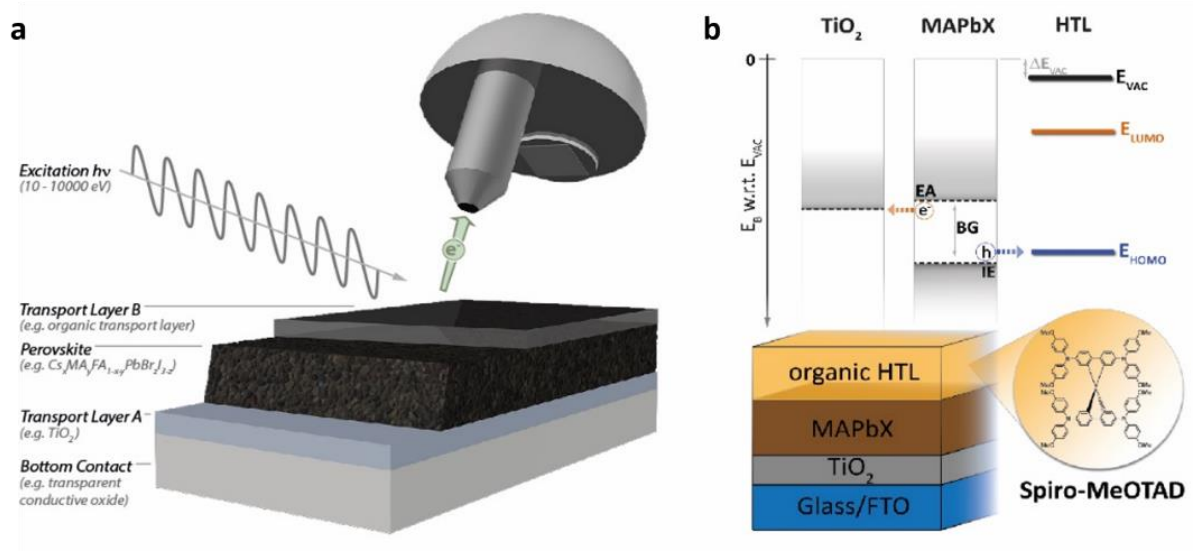

Figure 1. Photoemission spectroscopy of halide perovskite thin films. a) Schematic of the PES experiment for a typical perovskite thin film on top of a transport layer A. For the analysis of the forming interface incremental (typically 0.1 – 30 nm) overlayers of a transport layer B can be grown on top while successively performing the PES measurements. b) Energy level diagram for a typical halide perovskite solar cell stack. PES measurements give access to key energetic parameters, the formation of interface dipoles (ΔE_{vac}) and to adjacent transport layers (here: energies of the lowest unoccupied molecular orbital, E_{LUMO}, and highest occupied molecular orbital, E_{HOMO}, of an organic semiconductor).

Assuming the absence of additional chemical reactions, the determined values can be used as input parameters for transport models based on thermionic emission at HaP/metal interfaces, i.e. in the Mott-Schottky limit,[11] or equivalently for HaP-semiconductor heterojunctions described by the Anderson rule.[12] Thereby, the electronic structure of the interface is defined

by vacuum level alignment, and the interface energy barrier for electron and hole transport is the difference between the EAs and IEs of the two materials, respectively. We note that over the past decades expanded and more realistic models were developed for many semiconductor systems. Notably, the generation of these models also relied on the precise determination of the energy level alignment process between the two films and, for example, comprise interface dipole formation and induced density of interface state effects.[13–15]

New means and increasingly powerful computational methods for the calculation of the electronic structure of semiconductor surfaces and interfaces along with more accurate PES experiments were at the forefront of the development of these models. Particularly, *in situ* layer growth, to determine band onsets (i.e. the distance of the band extrema from E_F) at the surface and band offsets at the interface of two semiconductors by PES became a hallmark method for model validation.[16]

Following this path, we will lay out how PES, as the method of choice to measure E_{VBM}, IE and the densities of states (DOS) of frontier electronic states at the surface, can be employed for HaP systems. We note that, in this context, often inverse photoemission spectroscopy (IPES) is mentioned as a complementary tool to identify E_{CBM} and the EA. For further reading on the many interface systems that exist between HaP films and a large variety of functional layers (transparent conductive oxides, organic semiconductors, metal contacts, etc.) we point to a host of literature and review pieces that go beyond PES methods and reference further detailed studies.[17–20]

2.Methodology

2.1. Photoemission spectroscopy: working principle and measurements conditions

2.1.1.Working principle

PES can be commonly considered as a set of non-destructive analytical characterization tools based on the principle of photoelectric effect.[21,22] PES is usually performed under ultra-high vacuum (UHV) conditions and used to determine the chemical and electronic properties of the surface and near surface region of a (semi-)conductive sample, with the probing depth depending on the photon energy used for the generation of photoelectrons. In a classical picture, the photoemission process can be described as a three-step process, occurring almost simultaneously. First, the sample is irradiated with high energy photons (either from an X-ray tube, a gas discharge lamp, laser excitation or a synchrotron radiation source), which excite electrons via the photoelectric effect. Secondly, the excited electron travels though the solid towards the surface. While on its path to the surface, the electron can be subject to multiple scattering events and hence lose parts of its initial kinetic energy, which would eventually give rise to well defined background contribution in the captured (photo)electron distribution curve (EDC) from these so-called secondary electrons.[23–26] However, part of the excited electrons escape the solid without energy loss through the surface into UHV and are subsequently captured and detected in the spectrometer in the final step. These primary electrons are emitted with well-defined kinetic energies, which correlate to a first approximation with the corresponding binding energy the electrons had in their initial bound state in the solid.[27] In this way the electron provides insight into the nature and atomic level of the material it is emitted from and yield element and compound dependent signatures in the EDC.

Mathematically, the photoemission process can be expressed according to the Equation 1:[28]

$$E_K = h\nu - E_b - W \quad \textbf{(1)}$$

with, the measured kinetic energy E_K, the photon energy hν, the binding energy the electron had in the solid E_b, and the spectrometer work function W.

The incident photon energy determines the range of accessible binding energies of occupied states in the solid and hence the nature of the probed electronic energy levels, i.e. deep core

levels, shallow core levels or valence band electrons. As a final point concerning the working principle of PES, we note that the photoemission process generates, via the emission of a free electron, an atomic perturbation that is the photohole, i.e. a positive charge remaining on the surface. In a more involved theoretical description this photohole would be considered in the final state energy of the electronic systems.[27] Practically, this perturbation must be compensated by complex de-excitation phenomenon which needs to be considered accurately. Furthermore, as soon as the solid has poor electrical conductivity (charging) or (photo)chemical instabilities,[29] which can be the case for complex materials such as HaPs, de-excitation and charge compensation become a considerable challenge for the PES experiment.

2.1.2.Measurements parameters

Vacuum environment

Standard PES measurements are run under UHV conditions.[29] These measurement conditions are required since the UHV environment allows the analysis of pristine sample surfaces and for unperturbed trajectories of the photoelectrons through the spectrometer to the detector.

Thus, first UHV minimizes surface contamination of the probed sample. For reference, a perfectly clean surface (e.g. via sputter-anneal-cycles) is covered by a monolayer of CO molecules within 1 second at a background pressure of 10^{-6} mbar. Second, as electrons with low energy are easily scattered by the residual gas molecules, a good ratio between the noise and the total spectral intensity typically requires working at a pressure in the range of 10^{-8} to 10^{-10} mbar.[30]

We note in this context that due to the recent developments in vacuum equipment and spectrometer configurations for PES experiments, it is now possible to probe surfaces under more realistic environmental conditions, i.e. at higher pressure through Near Ambient Pressure PES (NAP-PES).[31] This method enables to track interactions between molecules in the gas

phase and the surface at a pressure of up to 20 mbar, by placing a sample inside a specific cell which is opened to the analyzer via a small aperture. For HaP semiconductors dedicated experiments that probe the interaction between the HaP surface and environmental gases, such as O_2 and H_2O, by NAP-XPS, can yield invaluable information on the degradation relevant in many device applications.[32,33]

Probing depth

Generally, the probing depth in a PES experiment is limited by the escape length of the photoemitted electrons, which is related to their inelastic mean free path (IMFP) in the solid and hence the corresponding kinetic energy of the electrons. This surface selectivity is a fundamental characteristic and strength of PES techniques, but also limits their applicability for the characterization of bulk properties.

The photoelectron IMFP describes the mean distance an electron of a specific kinetic energy can travel through the solid before it scatters inelastically, thereby losing energy to its surroundings.[34] Values for the IMFP were compiled by Seah and Dench [35] (Figure 2) and plotted in a "universal curve" that yields an estimate for the attenuation length of photoelectrons in various PES (and IPES) techniques. The actual probing depth amounts to approximately three times the IMFP, with more than 60% of the signal coming from within a distance of one IMFP from the surface.[29] Therefore, typically the probing depth will vary between 1 nm and 15 nm, depending on the PES technique used. It is however important to note that, in the low kinetic energy electrons range, the IMFP value is mainly dependent on the electron-phonon scattering, which will vary regarding the nature of the material. Thus, the depth analysis is highly material dependent and can vary by an order of magnitude.[27,36–38] Today, the most accurate values of IMFP are implemented according to the formula TPP-2M of Tanuma *et al*.[39]

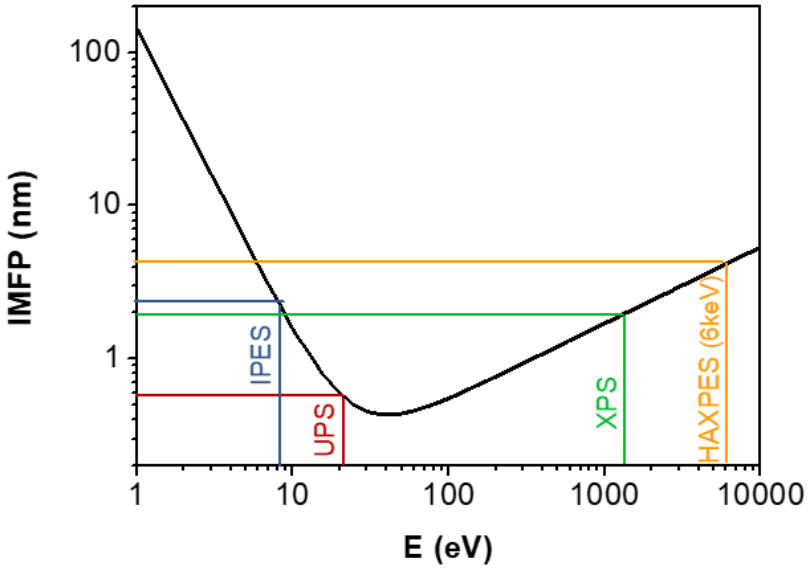

Figure 2. Inelastic mean free path (IMFP) of electrons in pure elemental materials as a function of the electron kinetic energy yielding the "universal curve" according to Seah and Dench. Adapted with permission.[35] Copyright 1979, American Chemical Society.

However, the IMFP parameter should not be the sole parameter employed for depth-resolved analysis since it only takes the effect of inelastic scattering into consideration. The implementation of the effective attenuation length (EAL), which includes the effects of both elastic and inelastic scattering, is one option to overcome this shortcoming. By including elastic scattering, the apparent depth of electrons can increase without inducing any change in energy, when layers of different electron densities are studied at off normal takeoff angles, due to modifications of the emitted angular distribution of electrons and thus, of the shape of energy spectrum distribution curve.[34,40]

Further quantitative assessment of vertical position of atom in the analyzer area can also be achieved by considering the energy loss during PES measurements. These losses are related to two origins, firstly due to the creation of core holes, and secondly due to the transition of the photoelectron as it moves toward to the surface.[41] Thanks to simulation software covering

these aspects,[42–44] it is possible to investigate the influences of surface texturing [45] but also vertical compositional information.[46]

2.2.Commonly Applied PES Techniques

Comprehensive descriptions and guidelines for the performance of PES measurements can be found in literature for a broad range of material systems in general[34] and halide perovskites in particular.[47] In this section we give a brief overview over the most common PES methods, that found widespread applications for the determination of chemical and electronic properties at HaP surfaces and interfaces.

2.2.1.X-ray Photoelectron Spectroscopy (XPS)

Among all PES techniques, XPS is the most commonly used, and is hence sourced exhaustively in existing reports and textbooks.[27–29,34,48] In XPS measurements, photoelectrons are excited by an X-ray source operating at excitation energies between 150-2000 eV, i.e. in the range of soft X-rays. We will discuss hard X-ray-based PES methods that offer a larger probing depth in separate subsections (sections 2.2.2 and **Erreur ! Source du renvoi introuvable.**). For standard XPS measurements the typical sources available in laboratories are based on Al or Mg anodes emitting Al Kα (1486.6 eV) or Mg Kα (1256.6 eV) radiation, respectively.

For each element present in the material under investigation, one or several photopeaks at specific energy (dependent on the core level) are observed within the recorded energy range. Except for H and He, all elements from the periodic table exhibit these characteristic core level photopeaks as “finger prints” which in turn allow the assignment of atomic components of the probed surface in the XPS analysis. Moreover, and with particular relevance for multicomponent HaP systems, the evolution of the chemical environment of the observed atomic species can be determined by tracking chemical shifts in the photoelectron binding energy (E_B).

For the analysis of the chemical composition, XPS serves as a quantitative tool as the photopeak intensities are proportional to the atomic concentration weighted by the energy level dependent photo-ionization cross-section σ. Values for σ are strongly depending on the kinetic energy, thus linked to the used excitation energy, but have been determined and tabulated for many core levels under standard XPS conditions.[27,29,34] Depending on the cross-section of the most prominent characteristic photopeak the detection limit in XPS can range down to 0.5% at.

The energy resolution of the spectra is critical for the precise determination of the electron's E_B and is dependent on the electron energy analyzer as well as the X-ray source.[48] By using monochromatic sources, one can obtain an energy resolution as low as 0.3 eV, providing thus a very accurate interpretation of the chemical environments in the probed region when dedicated fits to the spectra are performed. Concerning the spatial resolution, the analyzer spot size is now close to 10-30 µm for laboratory spectrometers and can reach down values within the range of micrometer (up to 1µm for Kratos instruments) for specific energy analyzer configurations.

XPS photopeaks nomenclature is based on quantum numbers and is widely documented in literature.[27,29,34,49] With the exception of the s orbitals (angular momentum quantum number l = 0), all orbital levels present a doublet, with a spin-orbit splitting (j = l + s), where the two possible states exhibit a different E_B for the two spin components.[49] Nowadays, spin-orbit splittings are well tabulated in literature [29] for all element core levels, which aids significantly for high resolution peak fitting.

2.2.2.Hard X-ray Photoemission Spectroscopy (HAXPES)

As mentioned in the preceding section, the probing depth for a classical laboratory spectrometer operated with Al or Mg X-ray source is limited to approximately 10 nm. Current trends in the advancement of XPS methods [50] focus on the use of radiation with higher excitation energies to extend the sampling depths in hard X-ray photoemission spectroscopy (HAXPES). This is

well illustrated by the universal curve for the electron IMFP and the corresponding energy range above 2 keV (Figure 2).

An initial reason to introduce HAXPES measurements has been to reduce the effect of surfaces, i.e. contamination, and capture more signal originating from the bulk of the probed materials.[51] In a systematic approach, the variation of the excitation energy lets us sample the composition at the surface and in the sub-surface region. For HaP films this approach is valuable as it offers insight into potential stoichiometric deviations due to the segregation of chemical species as will be discussed in section 3.4.

Hard X-rays can either be generated at synchrotron beam lines or also on a laboratory scale with the recent development of new sources. For example, by using the Ag Lα line (2984.2 eV) instead of the Al Kα (1486.6 eV), the information depth is extended to about 18 nm from the sample surface. However, sources yielding even higher photon energies (and thus extending the probing depth) become available such as X-ray anodes producing Ga Kα (9252 eV) radiation.

Generally, the type of data gained from HAXPES measurements is the same as in a regular XPS experiment, but some disadvantages amount to a loss in energy resolution as well as in the photoionization cross-section. Accurate data for photoionization cross-sections at high energy excitation are not as routinely available as for Al or Mg X-rays sources. Hence, the quantitative interpretation of core levels intensities remains ambiguous and requires careful calibration steps for new compounds and rarely probed core levels. Moreover, HAXPES techniques need to be performed with the caveat of potentially more pronounced beam damage of the samples than in soft X-ray methods. While the larger inelastic mean free path of high energy electrons implies fewer interactions with the material and thus integrally less beam damage, the potential for sample degradation is rather rooted in the nature of the typical radiation flux. HAXPES measurements are usually performed at synchrotron light sources, which exhibit a higher

brightness compared to laboratory-based X-ray sources. In order to achieve similar signal to noise ratios, spectrum acquisition is usually done with high X-ray flux in the analyzer spot. It is thus important to perform measurements with intensities which will not lead to a faster chemical degradation of HaPs (Pb0 growth for example) due to their high sensitivity (especially the photosensitivity).[52] Means to follow these precautions are to de-tune the monochromator of the incoming X-ray beam or use filters to attenuate the beam intensity particularly for lower order reflections in the range of soft X-ray which would otherwise accelerate sample degradation. Several examples show that HaP film formulations exist, that can provide high stability even under an excitation energy of 2100 eV.[53]

2.2.3.Ultraviolet Photoemission Spectroscopy (UPS)

In UPS measurements, samples are irradiated with ultraviolet photons, either from a discharge lamp (most commonly He I or He II emission at 21.2 or 40.8 eV, respectively) or by laser excitation or in the distant UV by synchrotron radiation. Analogous to the process in XPS measurements, the UV-excited photoelectrons are then collected to retrieve the EDC and hence the density of states.[48]

In practice, the energy resolution of the UPS experiment is on the order of 0.1 eV but can be as high as only a few meV in dedicated setups with highly monochromatic sources and low temperature conditions. This allows for a more precise determination of the valence band density of states, including the electronic states near the Fermi level. The spatial resolution is strongly dependent on the electron analyzer and photon source used, but can go down to 10 µm.[48] For the most common UPS measurement procedure using He I excitation (21.22 eV), the kinetic energy of electrons originating from the valence band onset and frontier occupied molecular orbitals is on the order of 15-20 eV. This principally makes standard UPS measurements more surface sensitive than their XPS counterparts, restricting analysis to the

very top layers of the studied surface. Thus, the avoidance of surface contamination becomes critical for an accurate characterization of the valence band features by UPS.

2.2.4.Inverse Photoemission Spectroscopy (IPES)

IPES is a surface sensitive method that is complementary to the PES tool box. In contrast to PES measurement, in IPES the sample is irradiated with low kinetic energy (5 – 50 eV) electrons. After entering the solid, the electrons dissipate their kinetic energy, either radiatively or non-radiatively, and reach states at lower energy. If this decay is radiative, the emitted photon can be detected.[54] As the initial energy of the electron is known, the measured energy of the emitted photon leads to the determination of the final state, which represents a previously unoccupied energy level above the Fermi level.[55] Thus, this spectroscopy technique unlocks access to the unoccupied density of states from the conduction band.[27]

Acquisition times in IPES measurements are longer than the UPS ones, due to a significantly lower count rate. The energy resolution can reach ~0.2 eV with a spatial resolution of around 1 mm.[55]

2.2.5.Angle-Resolved Photoemission Spectroscopy (ARPES)

For all PES measurements presented above, the photoemission is generally detected along the normal of the sample surface and via angle-integrating electron optics. The basic principle of ARPES is to vary the observed emission angle of electrons, either by tilting the sample, by moving the analyzer, or in a specific analyzer and detector configuration (p-ARXPS) , which is based on the simultaneous collection of the photoelectrons emitted under different angles without tilting the sample.[56]

Furthermore, area detectors enable the discrimination of emission angles for electrons within the acceptance cone passing through the analyzer optics.

By introducing angular resolution in XPS measurements, quantitative information about the depth distribution of the elements in the top few nanometers of the sample can be extracted, as one can reduces the effective escape depth of electron at emission under grazing angles. Performing HARPES (Hard X-ray Angle-Resolved Photoelectron Spectroscopy) presents a versatile approach to vary the surface contribution to the spectrum and obtain a more discriminate picture of the bulk and surface electronic structure and chemical composition.

Finally, angle-resolved UPS (ARUPS) measurements consist of acquiring several spectra at varied angles from a monocrystalline or highly ordered polycrystalline material, which leads to the generation of "band-maps" of the electronic structure of the valence bands, i.e. mapping of the dispersion relation.[48] Note that this analysis can also be pursued at higher photon energies, by working with hard X-ray excitation in HARPES mode. This provides a more bulk-sensitive electronic structure determination through angle-resolved band mapping, particularly attractive for *ex-situ* prepared samples, with surface contamination. It is however necessary to keep in mind that working in the hard X-ray regime can lead to specific issues, such as increased radiation damage.[57]

Clearly, coupling all these PES techniques is thus a comprehensive approach to obtain a complete overview of the chemical and electronic properties of materials. Hence, the surface chemical gradient inside the top material layer and its quantification can be easily determined at different probed thicknesses through a combined study with XPS, ARXPS and HAXPES measurements and will be detailed in section **Erreur ! Source du renvoi introuvable.**. with specific application to HaP materials.

2.3.Spectrometer calibration and the influence of charging effects

Recently, the issue of faulty data analysis in PES measurements has been raised by the research community, which highlights poor and incorrect material data analysis in the past.[58] The aim of this review is not to give a detailed guide about the execution of one specific PES

measurement, for which we rather refer to existing ASTM standards,[59–62] ISO standards[63–65] and additional literature,[34,66] especially for HaPs materials.[38,47] More specifically, Philippe *et al.*[38] recently detailed good practices regarding PES measurements for HaPs (sample preparation, calibration, radiation damages).

However, we would like to emphasize the question of charging effects during PES measurements since they can lead to important misinterpretations of PES data. We thus turn to a technical aspect that can become particularly relevant for the determination of the binding energy of core levels. In case of poorly conductive samples, which holds true for a subset of HaP compounds in the absence of photogenerated carriers over the entire sample structure, one can encounter erroneous photopeak positions due to charging. This charging effect is corresponding to photoholes that accumulate at the sample surface leading to a positive electrostatic potential. In consequence, photoelectrons leave the sample at lower kinetic energies. During XPS measurements, this charging effect hence leads to an apparent shift of the photopeaks to higher binding energies. Thus, charge compensation can become necessary for measurements in which electrostatic charging occurs. Usually charge compensation can be achieved by "flooding" the sample surface with an excess of low-energy electrons to balance out the positive charges.[29] This workaround enables that an elemental quantification can still be obtained in the case charge compensation is used for the measurement. Other methods are also available from literature, with specific focus on sample mounting.[34] However, we note that the identification of chemical environments becomes more difficult and needs to strongly rely on the analysis of core level peak positions relative to each other at best. In addition, the determination of band onsets is no longer possible, as the constant flow of electrons constitutes an arbitrary shift of E_F on the sample surface.

When reaching the determination of energetic diagrams, issues raised by the charging artefact become more critical. Indeed, in this case; charge compensation via flooding is not appropriate.

To overcome this issue, the sample preparation as well as calibration step (especially for UPS measurements) are key parameters and some examples can be found in literature.[34,38] It is also very important to corroborate the experimental data obtained through PES measurements with other experimental work to probe the validity of the energetic diagrams obtained. More details will be specified in Section 3.2.

3.PES analysis of HaP material properties

3.1.Stoichiometry and chemical composition

The stoichiometry measure by XPS is highly dependent on the chemical environment at the HaP surface, but the accuracy of the evaluation can be improved by an appropriate choice of photopeaks and the corresponding range of E_B. Indeed, the probing depth of the analysis varies depending on the chosen energy range. This effect is typical for system in which the surface composition deviates from the bulk composition and was for instance reported for other materials that find application in photovoltaic and other optoelectronic applications. For example, in the case of $Cu(In,Ga)Se_2$ solar absorber layers, the GGI key ratio ([Ga]/([Ga]+[In])) evolves from 0.25 to 0.29 depending on the energy range chosen for the photopeak analysis (ΔE_K = 675 eV if Ga $2p_{3/2}$ and In $3d_{5/2}$ levels are chosen and 10 eV if the Ga 3d and In 4d levels are chosen for the analysis, respectively), for a theoretical value of 0.30.[67] The larger the distance between the binding energy range of two or more probed elements, the larger is the variation in IMFP, which poses a predicament on the determination of the absolute stoichiometry.

The issue can be rectified by applying a kinetic energy dependent sampling depth correction, which however does not eliminate surface segregation or gradient effects. However, it is not always possible to access core levels with neighboring energy ranges for materials with complex stoichiometries such as HaPs. Indeed, as described in the following paragraph, wide

energy windows are involved for HaP materials, with at least an energy difference of 250 eV between the nitrogen and iodine core levels. Therefore, as there is a lack of better alternatives, recording the major photopeaks of the constituent elements, for which standard spectra are indexed in the literature, is the more advised strategy. In the following we give a few select examples of the most relevant elements probed for HaP analysis.

Multiple halide elements can be implemented for HaPs solar cells, the most common ones being I, Br and Cl. Numerous comparative studies of $MAPbX_3$ (where X represents the halide) absorbers can be found in literature,[8,9,68–70] enabling a more consistent indexation of the BE peak positions of the main core levels: I $3d_{5/2}$ (619.5 ± 0.1 eV), Cl $2p_{3/2}$ (198.5 ± 0.1 eV) and Br $3d_{5/2}$ (68.5 ± 0.2 eV). Those E_B can slightly evolve, especially for mixed cations such as $MAPbI_{3-x}Cl_x$ and $MAPbI_{3-x}Br_x$ (Table 1).[71–73]

The case of Pb is interesting because the corresponding E_B will be influenced by the halide element it is bound to. Indeed, for $MAPbI_3$ system, the Pb $4f_{7/2}$ photopeak is positioned at a E_B of 138.6 ± 0.1 eV but is shifted to 139.1 ± 0.1 eV in pure $MAPbCl_3$ or $MAPbBr_3$ structures.[9,68] For $MAPbI_3$ systems the binding energy range from 15 to 55 eV is suitable for a more accurate chemical analysis as it contains the Pb 5d and I 4d core levels (Pb $5d_{5/2}$ at 19.7 ± 0.1 eV and I $4d_{5/2}$ at 49.5 ± 0.1 eV), offering measurements at similar probing depth for both elements.[9]

In this context we note that lead can be substituted with tin. Liu *et al.*[74] studied the incorporation of Sn in mixed perovskites with different structures. For $CsSn_{0.6}Pb_{0.4}I_3$ quantum-dots, they found the Sn $3d_{5/2}$ E_B at 486.2 ± 0.1 eV. Kamarudin *et al.*[75] found that several oxidations states are attainable for Sn, with Sn^{4+} at 486.9 ± 0.1 eV, Sn^{2+} at 485.9± 0.1 eV and Sn^0 at 484.5± 0.1 eV in E_B for $FA_{0.98}EDA_{0.01}SnI_3$ structures. Furthermore, heterovalent substitutions of lead are attempted, for instance by Bi, to expand the class of perovskite-like materials.[76] The binding energy of the Bi $4f_{7/2}$ photopeak in $(CH_3NH_3)_3Bi_2I_9$ is located at 159.0 ± 0.1 eV. However, as the Bi 5s photopeak has a similar binding energy than the Bi $4f_{7/2}$ one

(159.4± 0.1 eV and 159.0 ± 0.1 eV, respectively), the best reference to index to $MABiI_3$ position becomes thus Bi $4f_{5/2}$, located at 164.3 ± 0.1 eV (spin orbit splitting of 5.3 eV).

For more complex structures such as triple cation mixed halide perovskites ($Cs_{0.05}(MA_{0.15}FA_{0.85})_{0.95}Pb(I_{0.85}Br_{0.15})_3$ and $Cs_{0.1}(MA_{0.15}FA_{0.85})_{0.9}Pb(I_{0.85}Br_{0.15})_3$ for example), where FA denotes organic formamidinium ($C(NH_2)_2$) cations, the literature remains sparse. For reference, the Cs $3d_{5/2}$ core level in this structure is located at 725 ± 0.1 eV.[69] This position slightly shifts for a different perovskite structure such as $CsSn_{0.6}Pb_{0.4}I_3$ quantum-dots where it is measured at 726.6 ± 0.1 eV, even though the Pb $4f_{7/2}$ and I $3d_{5/2}$ peak positions are found at their usual binding energy (138.5 ± 0.1 eV and 619.6 ± 0.3 eV respectively).[74]

Fitting the C 1s spectrum is complex and is ideally performed in correlation with the N 1s spectra fitting. Indeed, one would only expect the presence of C-N bonds, in MA^+ and/or FA^+, which have been well identified.[77,78] Jacobsson *et al.*[78] performed the deconvolution of the C 1s and N 1s spectra based on three different perovskites, using $MAPbBr_3$, $FAPbI_3$ and mixed perovskite $(FAPbI_3)_{0.85}(MaPbBr_3)_{0.15}$ (obtained by spin-coating). Specific E_B values for the C 1s were derived from their work, namely at 288.4 and 286.5 eV for the carbon in FA^+ and MA^+, respectively; the corresponding N 1s positions were determined at 400.8 and 402.5 eV, respectively, but were shifted by +0.2 eV in the case of mixed halide perovskite (Figure 3, a and b). Table 1 summarizes values for E_B and spin orbit splitting for the major core levels photopeaks of HaP materials.

Often, other contributions at lower E_B - between 285.4 eV and 284.6 eV - are observed in the C 1s region and have to be indexed according to their E_B. Jung *et al.*[77] attributed a contribution in this region to the presence of CH_3-NH_2 at 285.4 eV, in correlation with literature values.[79] They found this component for HaP films that were grown via two different deposition methods, either by spin coating of a PbI_2 layer followed by exposure to MAI solution [77] or by

a sequential vacuum evaporation process.[80] They assume this carbon contribution to be a structural defect at the interface between MAI and PbI_2, which disappeared after annealing. Another C 1s photopeak observed at 285.3 eV was attributed to the presence of CH_3I [81] which could arise from the thermal decomposition of MAI (Figure 3, c-e).[82] In addition, adventitious carbon can be present when films have been exposed to ambient or other environmental conditions that lead to inherent contamination. In this case, multiple additional components can be detected on the surface: C-C bond at 284.5 to 285 eV (depending on the initial calibration performed) due to the presence of hydrocarbons species in air,[83] but also oxygen-related species, for which carbon-oxygen bonds (i.e. C-O, C=O, C-OH, RCOOH…) yield signal in the energy range between 285.5 and 289 eV.[84,85] For the latter, the corresponding O contamination becomes also apparent by the detection of the O 1s core level at E_B of 532.3-532.8 eV. Attribution of the contribution of C 1s at low E_B is thus not always well-defined, and has to be performed with precautions.[82,86] In this context we note that the calibration of binding energy scale to adventitious carbon has been a subject of controversial discussion, as it grossly neglects insufficient Fermi level alignment between spectrometer and the probed sample surface.[87] Now, particularly in the case of hybrid HaP materials and the corresponding multi-component carbon signal, we highly discourage the use of this referencing method.

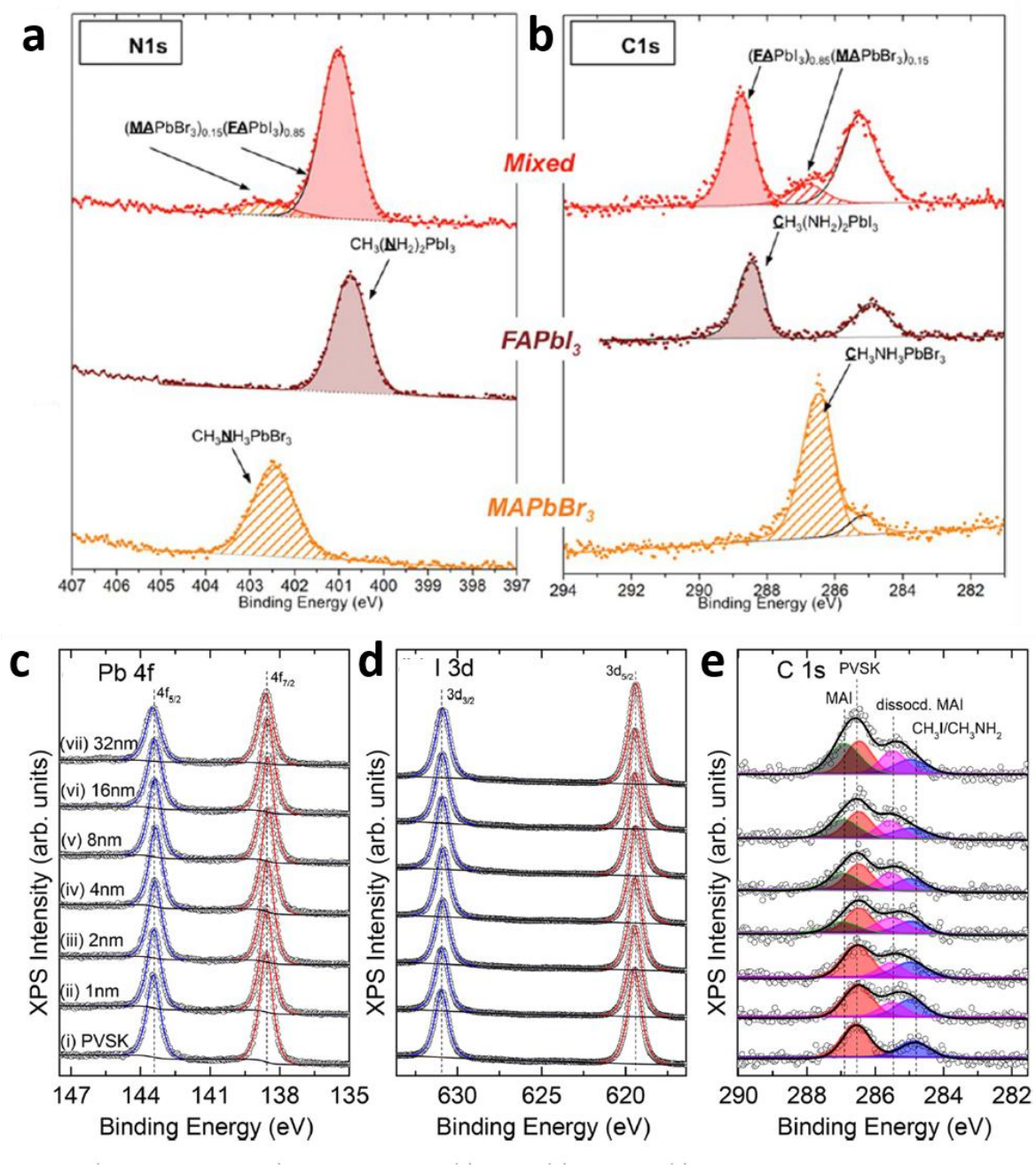

Figure 3. a) and b) N 1s and C 1s core level spectra (respectively) of the $(FAPbI_3)_{0.85}(MaPbBr_3)_{0.15}$, $FAPbI_3$ and $MAPbBr_3$ deposited on amorphous SnO_2/FTO substrates. Reproduced with permission.[78] Copyright 2016, American Chemical Society. c), d) and e) Pb 4f, I 3d and C 1s core level XPS spectra (respectively) of the $MAPbI_3$ film (i) and the samples after depositing an additional excess MAI layer of 1 (ii), 2 (iii), 4 (iv), 8 (v), 16 (vi), and 32 nm (vii). Reproduced with permission.[82] Copyright 2017, American Chemical Society.

Table 1. Characteristics of the main core level photopeaks of HaPs: E_B (eV) and spin orbit splitting (eV).

Core level	Attribution	E_B [eV]	ΔE Spin orbit splitting [eV]	References
I $3d_{5/2}$	$MAPbI_3$	619.5 ± 0.1	11.5 ± 0.1	[8,9,68]
	$MAPbI_{3-x}Cl_x$	619.5 ± 0.1	11.5 ± 0.1	[9,73]
	$MAPbI_{3-x}Br_x$	619.4 ± 0.1	11.5 ± 0.1	[73]
	$FAPbI_3$	619.2 ± 0.1	11.5 ± 0.1	[88]
	$CsSn_{0.6}Pb_{0.4}I_3$	619.6 ± 0.1	11.5 ± 0.1	[74]
Cl $2p_{3/2}$	$MAPbCl_3$	198.5 ± 0.1	1.6 ± 0.1	[9]
	$MAPbI_{3-x}Cl_x$	198.9 ± 0.1	1.6 ± 0.1	[72,89]
Br $3d_{5/2}$	$MAPbI_{3-x}Br_x$	68.8 ± 0.1	1.0 ± 0.1	[73]
	$(FAPbI_3)_{0.85}(MAPbBr_3)_{0.15}$	68.7 ± 0.1	1.0 ± 0.1	[90]
Br $3p_{3/2}$	$MAPbBr_3$	182.4 ± 0.1	6.7 ± 0.1	[68]
Pb $4f_{7/2}$	$MAPbI_3$	138.6 ± 0.1	4.8 ± 0.1	[8,9,68]
	$MAPbI_{3-x}Cl_x$	138.6 ± 0.1	4.8 ± 0.1	[9,73]
	$MAPbI_{3-x}Br_x$	139.0 ± 0.1	4.8 ± 0.1	[73]
	$FAPbI_3$	138.5 ± 0.1	4.8 ± 0.1	[88]
	$MAPbCl_3$	139.1 ± 0.1	4.8 ± 0.1	[9]
	$MAPbBr_3$	139.1 ± 0.1	4.8 ± 0.1	[73]
	$CsSn_{0.6}Pb_{0.4}I_3$	138.5 ± 0.1	4.8 ± 0.1	[74]
Pb $5d_{5/2}$	$(FAPbI_3)_{0.85}(MAPbBr_3)_{0.15}$	19.9 ± 0.1	2.6 ± 0.1	[90]
	$MAPbI_3$	19.7 ± 0.1	2.6 ± 0.1	[9]
Sn $3d_{5/2}$	$CsSn_{0.6}Pb_{0.4}I_3$	486.2 ± 0.1	8.4 ± 0.1	[74]
Bi $4f_{5/2}$	$MABiI_3$	164.3 ± 0.1	5.3 ± 0.1	[76]
Cs $3d_{5/2}$	$Cs_x(MA_{0.15}FA_{0.85})_{1-x}Pb(I_{0.85}Br_{0.15})_3$	725.0 ± 0.1	14.0 ± 0.1	[69]
	$CsSn_{0.6}Pb_{0.4}I_3$	726.6 ± 0.1	14.0 ± 0.1	[74]
C 1s	MA^+	286.5 ± 0.1	/	[78]
	FA^+	288.4 ± 0.1	/	[78]
N 1s	MA^+ a)	402.5 ± 0.1	/	[78]
	FA^+ a)	400.8 ± 0.1	/	[78]

a)(Positions are shifted by +0.2 eV in the case of mixed halide perovskite)

3.2.Energy levels and electronic structure

As laid out in the introduction, PES gives access not only to the chemical but also to the electronic properties of a material. Before describing the detailed process of characterizing the electronic properties, and thus the energy level alignment (ELA) at the interface, we briefly recap some important parameter definitions concerning the electronic properties of a surface that had been introduced earlier.

The first two important reference energies necessary to assess the position of electronic levels are the Fermi level (E_F) and the vacuum level (E_{VAC}), which were introduced earlier. E_F represents the energy at which the probability of occupation of an electronic state is ½ and is hence inherently linked to the electronic structure and electrochemical potential of the material investigated. For metals, E_F cuts through the conduction band and marks the limit between occupied and unoccupied states, while for an intrinsic or non-degenerately doped semiconductor, E_F is located within the band gap. E_{VAC} represents the energy threshold an electron needs to overcome in order to escape from the solid into vacuum. The work function (WF) represents thus the difference between those two values, according to the Equation 2:

$$WF = E_{VAC} - E_F \quad \textbf{(2)}$$

Similarly important are the distance between VBM and E_F as well as the distance between CBM and E_F, defined as the onset energies, E_{VBM} and E_{CBM}, respectively. These quantities are linked to the position of the Fermi level in the gap and hence the doping of the probed surface. They are directly related to IE and EA by the following equations 3 and 4:

$$E_{VBM} = IE - WF \quad \textbf{(3)}$$

$$E_{CBM} = WF - EA \quad \textbf{(4)}$$

A thorough investigation of these electronic properties to study the ELA in complex heterostructures can be achieved by a combination of XPS (position of the valence band maximum with respect to the Fermi level),[91] UPS (electronic density of states in the valence

band region, work function),[92] and IPES (position of the conduction band onset relative the Fermi level)[54] measurements.

It is important to note that the values obtained through PES measurements should always be compared to other experiments in order to validate the absence of any charging effect. Optical measurements as well as theoretical band gap predictions can be a good lead to compare the data obtained,[93,94] as well as a more recently developed technique named chemically resolved electrical measurements (CREM), developed by Cohen and coworkers.[95,96] For CREM, charging effects are consistently being followed and subsequently accounted for, to allow for the construction of a realistic band diagram for multi-interfacial structures. Another promising approach is the performance of operando PES measurements, which has been successfully demonstrated by Teeter *et al.*[97] for chalcopyrite solar cells. The authors find that photoexcitation due to x-rays or stray visible light during XPS or similar measurements can produce measurable photovoltages in materials, and thus, improve band-offset determinations with more reliable values for the junction built-in voltage.

A first complete description of the ELA in HaPs solar cells as measured by a combined PES/IPES approach was reported by Schulz *et al.*, in conventional as well as inverted device geometry.[10,98] Since then, the community explored more meticulously the electronic properties in general, and the band edge determination leading to the correct energy level assessment by PES/IPES in particular, which is topic of several reviews.[6,20,99,100] Note that the choice of the PES method employed can be critical when evaluating the intrinsic electronic properties of the perovskite surface. When perovskite films have been exposed to ambient air, the determining E_{VBM} by XPS is more precise than by UPS,[101] as UPS is more surface-sensitive and thus, more susceptible to inherent contamination. Apart from the ELA assessment, more recently complete band structure measurements of single crystalline HaPs were obtained, for $MAPbI_3$ and $MAPBr_3$ by ARPES experiments to refine the band onset determination.[102–106]

Looking back at typical values of ELA in HaPs, we begin with the study by Schulz *et al.*,[98] in which they investigated films with different compositions and provided first complete energy level positions for $MAPbX_3$ films (X = I, Br, $I_{3-x}Cl_x$) on top of TiO_2 bottom layers with and without thin evaporated HTLs as overlayer. Through the combination of UPS and IPES measurements, they obtained WFs of 4.0 eV for $MAPbI_3$ and $MAPbBr_3$ and 4.1 eV for $MAPbI_{3-x}Cl_x$, IEs of 5.4 eV for $MAPbI_3$ and $MAPbI_{3-x}Cl_x$ and 5.9 eV for $MAPbBr_3$, EAs of 3.7 eV for $MAPbI_3$ and $MAPbI_{3-x}Cl_x$ and 3.6 eV for $MAPbBr_3$ and electronic gaps of 1.7 eV for $MAPbI_3$ and $MAPbI_{3-x}Cl_x$ and 2.3 eV for $MAPbBr_3$ (Figure 4). The electronic gap values from combined UPS and IPES were assessed by comparison with optical measurements and density functional theory (DFT) calculations including spin-orbit coupling and GW approximation. Hence, the absence of charging allowed for an accurate determination of the band onsets for the study performed by Schulz *et al*.[98]

In order to assess the ELA to an adjacent HTL, the corresponding organic semiconductor is deposited on top in incremental steps, leading to a gradual buildup of the interface. This procedure has been pursued for the commonly employed HTL material N2,N2,N2′,N2′,N7,N7,N7′,N7′-octakis(4-methoxyphenyl)-9,9′-spirobi[9H-fluorene]-2,2′,7,7′-tetramine (spiro-MeOTAD) in the study by Schulz. The measurements indicate that vacuum level alignment occurs at this particular interface between HaP and spiro-MeOTAD, leading to an apparent offset between E_{VBM} in the HaP and the E_{HOMO} of the spiro-MeOTAD layer, which does not cause a barrier for hole extraction from the HaP to the HTL, but could in principle pose a limit to the attainable photovoltage. This initial PES investigation of this interface system led to further studies which indicate that the valence band offset in the ELA has no major impact on the device performance as long as the IE of the HTL is smaller than the IE of the HaP film.[6,107,108] Endres and co-workers [109] also performed similar experiments on $MAPbI_3$, $MAPbBr_3$ and $CsPbBr_3$ layers on top of TiO_2/FTO substrates and

combined the approach with a density functional theory (DFT)-based theoretical calculation of the DOS. In that work they corroborated the values obtained by Schulz *et al.*[98] for $MAPbI_3$ and $MAPbBr_3$ by a refined fitting procedure for the band edges (see section 4.2).

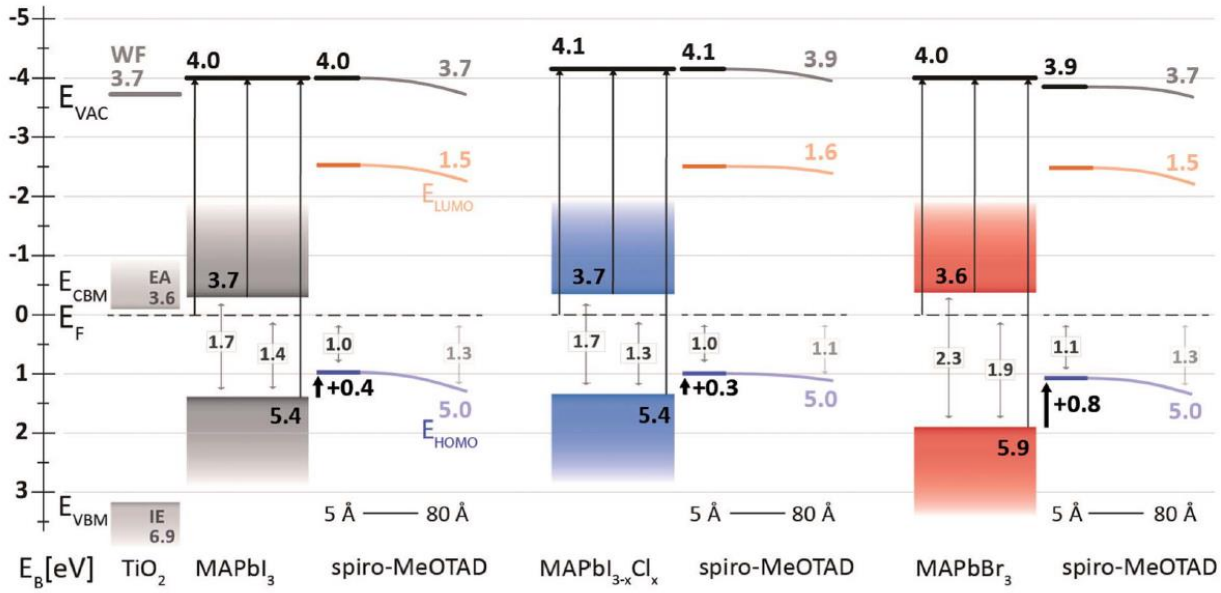

Figure 4. Experimentally determined energy level diagrams of interfaces between spiro-MeOTAD and MAPbX (X = I_3, $I_{3-x}Cl_x$, Br_3) on TiO_2. Each diagram provides the perovskite band gap, Fermi level position, electron affinity, ionization energy and work function. The HTL HOMO and LUMO positions with respect to the perovskite VBM and CBM underline key points of hole extraction and electron blocking, respectively. Minor band bending is observed throughout the spiro-MeOTAD film. Reproduced with permission.[98] Copyright 2014, Royal Society of Chemistry.

Recently, Olthof and her co-workers [110] performed a systematic study of the energy level positions in tin- and lead-based HaPs, by exploring the electronic properties of 18 different AMX_3 perovskite structures, through the variation of monovalent cations (A = FA^+, MA^+ or Cs^+), metal cations (M = Pb^{2+} or Sn^{2+}) and halide anions (X=I^-, Br^- or Cl^-). The study aimed at

a better understanding of the changes in the band gaps as well as the influence of composition on the absolute positions of VBM and CBM as measured by PES/IPES. The findings consistently track the increase in band gap energy with changing halide species, going from I to Br to Cl, in accordance with optical measurement and ab-initio calculations. Hence, CBM energy is shifted upward while a downward shift is observed for the VBM; both shifts correlate with the electronegativity and the metal to halide bond distances decrease (again from I to Br to Cl in decreasing order). The IEs and EAs of Sn-based perovskites are lower than those of their Pb-based counterparts, which is attributed to the lower electronegativity of Sn compared to Pb. As for the monovalent A-site cation, Olthof *et al.* report on a more convoluted trend in the change of the absolute IE and EA values, which they ascribe to a subtle interplay of the structural parameters on the unit cell scale (Figure 5, a).

Mixed halide perovskites also present an interesting trend in the electronic structure with regard to their single halide perovskite counterparts, as measured by PES. Li *et al.*[111] studied the influence of the halide nature, by tuning its composition in $MAPbX_3$ ($MAPbCl_3$, $MAPbBr_3$, $MAPbI_3$, $MAPbBr_{1.5}Cl_{1.5}$, $MAPbI_{2.1}Br_{0.9}$ and $MAPbI_{2.1}Cl_{0.9}$). The partial substitution of I by Br or Cl ($MAPbI_{2.1}Br_{0.9}$ and $MAPbI_{2.1}Cl_{0.9}$) leads to a fine control of the electronic properties, characterized by intermediate band onsets between those of the single halide perovskites (Figure 5, b). These dedicated PES/IPES studies are a first important step towards compiling a library of energy levels and have to be extended to other mixed HaPs.

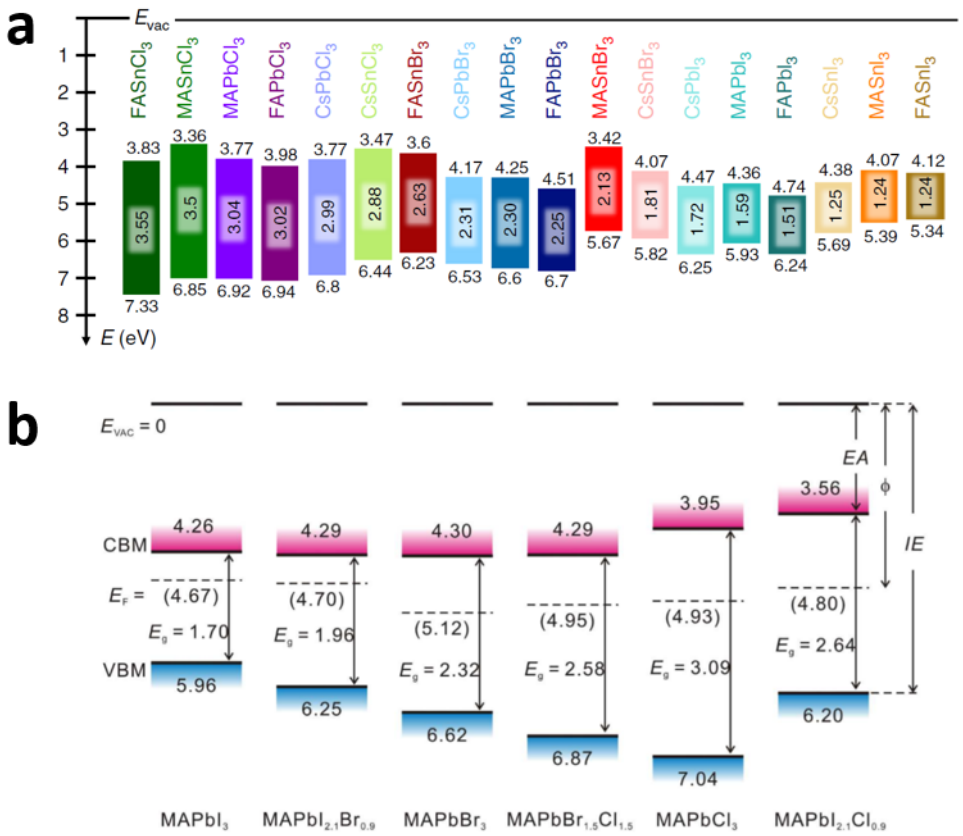

Figure 5. a) Schematic energy level diagram of 18 HaPs, with variations of monovalent cations, metal cations and halide anions with the respective IE, EA and band gap values. Reproduced with permission.[110] Copyright 2019, Springer Nature. b) Schematic energy level diagram of six metal halide perovskites, with variations of halide anions with the respective IE, EA and band gap values. Reproduced with permission.[111] Copyright 2016, American Chemical Society.

3.3.Reproducibility and reliability

Various deposition techniques for HaP thin film formation [4,81,112–120] as well as a variety of device architectures, *i.e.* conventional [100,121–124] or inverted [125–131] devices with a diverse selection of electron transport layer (ETL) or hole transport layer (HTL) have been realized to optimize device performances. It is noteworthy that the various deposition techniques and different sample architectures of HaP thin films induce a substantial variability of the PES

results for stoichiometric quantification and electronic properties. As an example, in literature, the electronic parameters values of $MAPbI_3$ vary significantly, with, for example, IE values ranging from 5.1 to 6.6 eV.[98,101,132–137]

3.3.1.Preparation method

Wang *et al.*[138] studied the effect of five different deposition techniques on the surface composition of $MAPbI_3$ deposited on Si substrates by XPS. They showed that the composition varies from one deposition technique to another, mainly in the carbon content, and related these variations to the dissociation of $MAPbI_3$ during the film formation.

Emara *et al.*[139] tried to correlate the electronic properties of $MAPbI_3$ films with the device efficiency of corresponding perovskite solar cells. They performed a UPS study on 40 $MAPbI_3$ films prepared with various methods and concluded that varying the preparation conditions leads to a wide range of electronic properties as the IE values were scattered within a range of 0.8 eV, which they attribute to fluctuations in the Pb/N ratio.

In a similar study, Wang *et al.*[138] report on a dependence of the work function on the deposition method, yet the spread in observed IEs is less pronounced than in the study of Emara *et al.*[139] Note that, for both studies, the evolution of electronic structure and properties is correlated with the evolution of the surface stoichiometry (assessed by XPS). These examples demonstrate that PES is a powerful tool to correlate surface composition and energetics of HaPs. They also tell a cautionary tale that one needs to expect high sample-to-sample variance and ambiguity in the measured surface electronic properties, that can depend on minutia in the sample production process and despite other metrics (e.g. corresponding device characteristics) remaining mostly unaffected.

Sun *et al.*[140] used XPS mapping for laterally resolved chemical analysis of MAPbI3 thin films to probe the influence of sample preparation parameters. They studied three different deposition methods[117,141,142] and plotted the spatially resolved maps of the I/Pb ratio for each sample.

Imaging XPS techniques are of primary interest to investigate the surface homogeneity.[143] The main challenge is to combine sufficient data collection in a limited amount of acquisition time [144] with the minimization beam damage to the HaP layers. Here, Sun *et al.*[140] demonstrate that the I/Pb ratio is not homogenous within the deposition method but also from one batch to another as well as within the same sample (Figure 6).

The work denotes a proof of concept regarding mapping of perovskite layers but reveals two critical challenges in the data analysis and correlation. The first issue is related to the discrepancy of the I/Pb ratio compared to expectation and literature values. Indeed, Sun *et al.*[140] present ratios within the range of 3.1 up to 4.1, not representative of a $MAPbI_3$ surface. It could be explained by an excess of MAI component since, as it will be detailed in Section 4.1.2, during storage under UHV, the I/Pb values decreases due to a loss of MAI surface adsorbents. The second issue concerns the origin of the lateral segregation within a similar sample. The strong variations in the I/Pb ratio can be induced by non-uniform coverage of surface contaminating species. Indeed, as no specific information is provided for the surface composition except the evolution of I/Pb ratio, it is reasonable to imagine that contamination could also be responsible, as well as the different options offered by the authors (concentration of solvent vapor, annealing temperature…). A critical cross-examination of this hypothesis would require at least the elemental maps of C, N and O species.

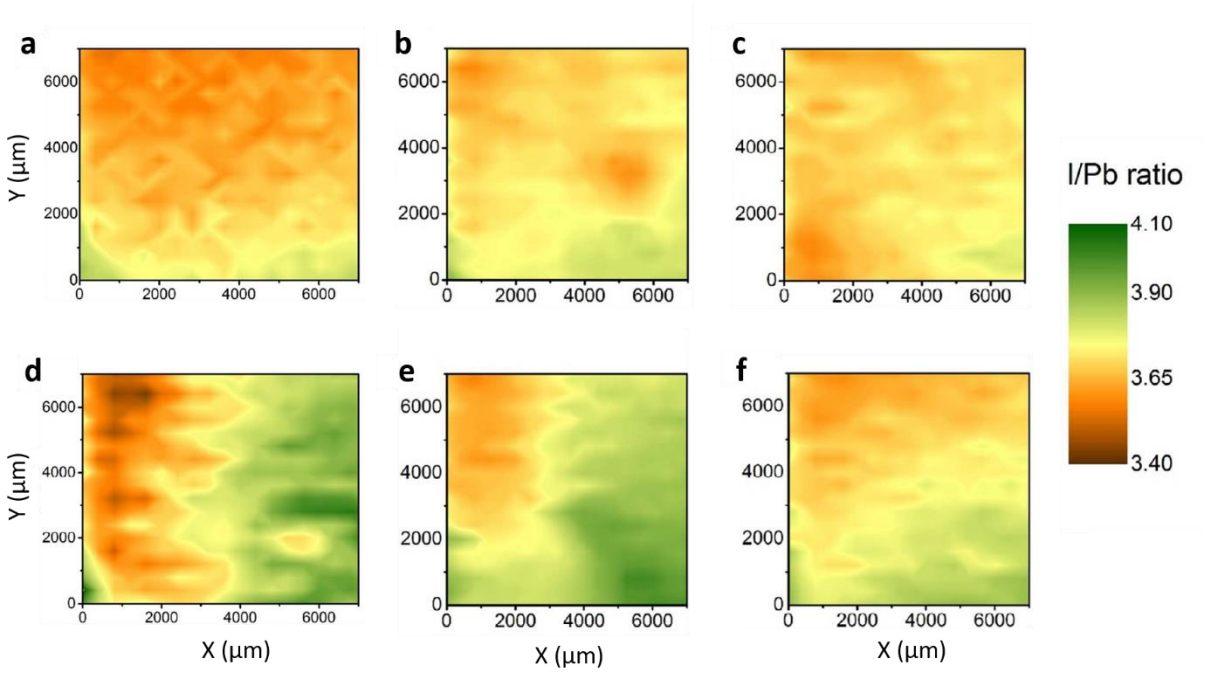

Figure 6. Homogeneous (a, b and c) and inhomogeneous (d, e and f) I/Pb maps of $MAPbI_3$ films deposited by different techniques according to Zhang's procedure (a, d)[142], Ahn's procedure (b, e)[117] and Jeon's procedure (c, f)[141]. Adapted with permission.[140] Copyright 2018, American Chemical Society.

3.3.2.Substrate influence

Further variations in the obtained PES results can be linked to the influence of the substrate, the HaP film is grown upon. Olthof and Meerholz [86] addressed the influence of the substrate type by depositing $MAPbI_3$ following a co-evaporation process on four different substrates: Indium doped tin oxide (ITO), MoO_3, PEDOT PSS (poly(3,4-ethylenedioxythiophene) polystyrene sulfonate)) and polyethylene ethoxylate (PEIE). After a thickness of over 30 nm has been deposited, all $MAPbI_3$ samples presented similar surface composition as determined in PES measurements. However, below a thickness of 30 nm, the surface composition and the growth mechanism appeared to be strongly substrate-dependent, with the formation of a PbI_2-rich phase at the reactive oxide interfaces.[6]

Most importantly, the influence of the substrate can result in a significant change in the electronic properties of the HaP surface even at several hundreds of nanometers distance from the buried interface. By exploring different n-type substrates (TiO_2, ZnO, ZrO_2, and F:SnO_2 (FTO)) and p-type substrates (PEDOT:PSS, NiO and Cu_2O), Miller and co-authors [101] found that the substrate types apparently change the electronic properties of thin $MAPbI_3$ layers, specifically their doping type. This trend was confirmed by Schulz *et al.*[10] who investigated several 100 nm's thick layers of $MAPbI_3$ on NiO and TiO_2 substrates and highlighted a work function shift of 700 meV, along with shifts of all the energy levels, depending on the substrate. This substrate dependency of the electronic properties of HaPs is further discussed in section 4.3, where we contrast the effect to potentially related phenomena such as Fermi level pinning and band bending.

3.4.Ageing and degradation

3.4.1.Modifications due to photon irradiation

The characterization of perovskites by PES, as well as their actual operation as light-harvesters in photovoltaic devices, obviously involves the exposure to electromagnetic radiation. It has been recently reported that surface photovoltage (SPV) of up to 0.7 eV can develop in an HaP film by varying the exciting UV photon flux during the UPS experiment in standard laboratory conditions.[145] The photovoltage buildup is related to the creation of electron-hole pairs upon UV excitation, which can substantially compensate the band bending at the surface of the perovskite films. Such an effect is critical to the measured E_B and should be considered when assessing PES results.

The effect of actual operating conditions on perovskite films embedded in a solar cell configuration was analyzed by XPS in vacuum.[146] The perovskite layer did not exhibit any significant change in its core level spectra after up to 15 hours of X-ray irradiation without any

additional illumination. However, exposure to additional white light led to degradation, characterized by the formation of metallic lead (Pb^0), as also highlighted in several PES studies on halide-based perovskites.[90,147,148] Indeed, the degradation of lead-iodide based perovskite has been proposed to involve the formation of PbI_2 and the segregation of the latter into metallic lead and I_2 by photolysis,[149,150] while a more intricate pathway for Pb^0 formation is linked to a Lewis acid base reaction centered on the de-protonation of the (organic) cation on the perovskite A-site.[151,152] This process is further described in section 4.1.1. Interestingly, this degradation into Pb^0 appeared to be strongly constrained upon the application of a voltage bias.[146] Thus implying that HaPs are more stable under voltage application, which could, for instance, suppress electrochemical processes.

However, a further study reports on a significant change in composition to readily occur upon X-ray exposure.[8] At an early stage of the exposure and up to 4.5 h of exposure, this change is characterized by the generation of iodine (I) and methyl ammonium (MA) vacancies, V_I and V_{MA}, respectively. Steirer *et al.* assume that these vacancies act as self-compensating defects that compensate each other and thus do not affect the position of valence and core levels yet. This could thus reflect on the proposed defect tolerance of perovskites at earlier stage of irradiation and explain the negligible X-ray beam damage assessed from XPS studies.[32] Nevertheless, over several hours of X-ray exposure the surface composition changes, with loss of methyl ammonium and iodine , corresponding to the degradation of $MAPbI_3$ into PbI_2.[8] In a comparable study, overnight exposure to X-rays in UHV of $MAPbI_3$ perovskite resulted in the degradation of $MAPbI_3$ to PbI_2 and Pb^0.[153] It is noteworthy that the light-induced degradation is insignificant in nitrogen-filled environment and mostly occurs when performing the illumination under vacuum conditions or in environments with oxygen content as low as 1 %.[148,154]

In summary, light and radiation exposure can damage the HaP film and even more so its surface, particularly under vacuum conditions. This (beam)damage effect can severely affect the results obtained in the XPS experiment and hence requires a careful measurement approach. Ideally spectra are recorded over short acquisition times and at reduced beam intensities to dynamically track changes that can occur during the measurement. To date the actual radiation impact or energy flux on the analyzed spot on the sample is rarely mentioned in the literature reports. Given the strong variation in HaP film stability, this induces another parameter of uncertainty in the comparison of completed studies. As a measure of best practice the radiation impact on the sample as well as transient behavior in the PES data should be reported similar to the procedures presented above.[8,147]

3.4.2.Thermal degradation

Since several heating steps (annealing step, module encapsulation…)[155] can be necessary for the fabrication of the HaP-based optoelectronic devices, understanding thermal degradation is thus of paramount importance and can be aided by dedicated PES experiments.

Investigations about thermal stability were performed by several groups, mostly on $MAPbI_3$-based samples.[156,157] For this compound, the chemical changes induced by thermal stress appeared at a nominal temperature of 130°C, through the decrease of the N 1s and the I 3d XPS signals, and in some cases, the growth of Pb^0 signal. The study explains this evolution by the $MAPbI_3$ decomposition into CH_3I, NH_3 and PbI_2, with the evaporation of CH_3I and NH_3 while PbI_2 remains on the surface. This thermal degradation process was claimed to progressively occur from the film surface to its bulk, already occurring when the material was exposed to 80 °C for extended time (>60 min).[157]

Very few literature reports exist about the deviation of electronic properties due to thermal degradation. Foley and co-authors [158] studied the evolution of $MAPbI_3$ electronic structure over a temperature increase from 28°C to 85°C. They reported no specific change in the

measured work function but observed a reversible shift in the VBM onset. In their review, Wang *et al.*[138] proposed a specific mechanism that would pertain to a potential evolution of the ELA. The model is based on an increase of PbI_2 degradation product, which presents different electronic properties compared to $MAPbI_3$ (IE of ≈ 6.3 eV and ≈ 5.3 eV for PbI_2 and $MAPbI_3$, respectively).

Note that combining thermal degradation and X-ray exposure during heating has also been reported to additionally contribute to the generation of Pb^0.[9]

3.4.3. Interfacial degradation

The long term stability of HaP devices is strongly related to interfaces,[6] where many different reactions can occur, leading to degradation of perovskite absorber and thus, to the change of its electronic and optoelectronic properties. A particularly unstable interface is the metal/HaP junction. In the classical device, perovskites films are often separated from any metal cell terminal through buffer and transport layers and are hence not directly in contact with the metallic species. However, different processes [6] can lead to the creation of metal HaP interfaces, notably metal migration from the contacts through the transport layer directly to the perovskite films,[159] pinholes formation inside the transport layer or more directly, via a deliberate cell design (HTM-free PSC).[160,161]

The presence of such an interface can lead to major implications for the HaP chemical state as proved by Zhao *et al.*[162] When exposed to different metals, they report the $MAPbI_3$ surface to spontaneously degrade through either redox chemistry reactions (Al, Ag, Cr and Yb) or partial charge transfer (Au). They evidenced this degradation through the appearance of a Pb^0 photopeak at 136.5 eV, without the presence of oxygen or light. This degradation is not specific to hybrid perovskites since degradation is also present for inorganic perovskites such as $CsPbI_3$ and $CsPbBr_3$.

Liu *et al.*[132] monitored the evolution of $MAPbI_3$ electronic properties by UPS upon incremental deposition of Au on top of $MAPbI_3$. After the first 0.5 Å Au deposition, a vacuum level shift of 0.3 eV (from 4.7 eV for pristine $MAPbI_3$ to 4.4 eV with 0.5 Å Au on top) is observed, possibly due to charging of Au particles from island-like growth on top of the HaP until a fully interconnected layer is formed. As more Au is deposited, a finite density of valence states is observed within the gap of $MAPbI_3$, until a true metallic Fermi edge is completely developed (Au thickness of 64 Å). Those two studies about perovskite/metal interface formation differ through the degradation process, as no degradation products (Pb^0 particularly) are seen in Liu's work.[132]

Ramos *et al.*[163] evaluated the impact of a Al_2O_3 encapsulation layer on $MAPbI_3$ surface chemical composition after deposition by atomic layer deposition. They accessed the chemical environment and composition of $MAPbI_3$ surface by depositing only 2 nm of Al_2O_3 at 60°C and 90°C. By monitoring the elemental ratios Pb/I and N/Pb they claimed that no significant surface modifications were induced during the Al_2O_3 encapsulation process performed at 60°C while at 90°C, after the Al_2O_3 layer deposition, the increase of the Pb/I ratio suggested the formation of a PbI_2-riched phase.

3.5.Tracking phase segregation and ion migration

The prevalence of ion migration and phase segregation in halide perovskite has been reported on extensively [164] and was linked to a unique combination of mechanical properties in HaPs.[2] In devices, ion migration affects transient behavior and can play into hysteresis effects as seen for PSCs.[165,166] Depth-profiling XPS can thus be a potent complementary characterization tool to explore and spatially resolve these compositional changes that originate from ion migration events.

Generally, time of flight secondary ion mass spectrometry (TOF-SIMS) is one of the most efficient characterization methods [167,168] to assess the above-mentioned ionic migration and HaP de-mixing. However, as the use of ion beam sputtering leads to accumulated damage of the investigated film,[169] access to the vertical distribution of the elemental components in the HaP film by PES, either with similar sputtering methods or via photon energy tuning, i.e. through HAXPES measurements, presents an alternative analysis to improve the consistency of determining compositional variations.

.

3.5.1.Depth profiling via sputtering

Several groups [170–172] already explored the chemical distribution of perovskite constituent elements by means of depth-profiling XPS analysis, which can be conducted based on two different sputtering methods, either by single ion or cluster ion sources.[50] The choice of the ion source for sputtering is intricate as HaPs are often hybrid organic inorganic compounds, and each ion source is optimized for sputtering either soft or hard materials. With a classical Ar^+ ion beam, as for ToF-SIMS, damages such as Pb^0 generation can be observed. The alternative, clusters of Ar ions (from few hundred to few thousand atoms), operate at reduced energy and hence are supposed to induce less damage. To assess the best sputtering conditions, Busby *et al*.[170,173] performed a systematic study of the evolution of the Pb^0/Pb ratio under different conditions, such as beam type, cluster size and kinetic ion energy, on pristine HaP films and full HaP solar cells (Figure 7). In their study they found 1 keV to be the best condition for profiling HaP layers with a monoatomic ion source. They also performed tests with ion clusters, for which they obtained the best, i.e. least perturbed, results with a few hundred atoms clusters, with an energy-per-atom value of about 20 eV. For smaller energy-per-atom ratios (<20 eV) they reported an artificial accumulation of metallic Au and Pb.

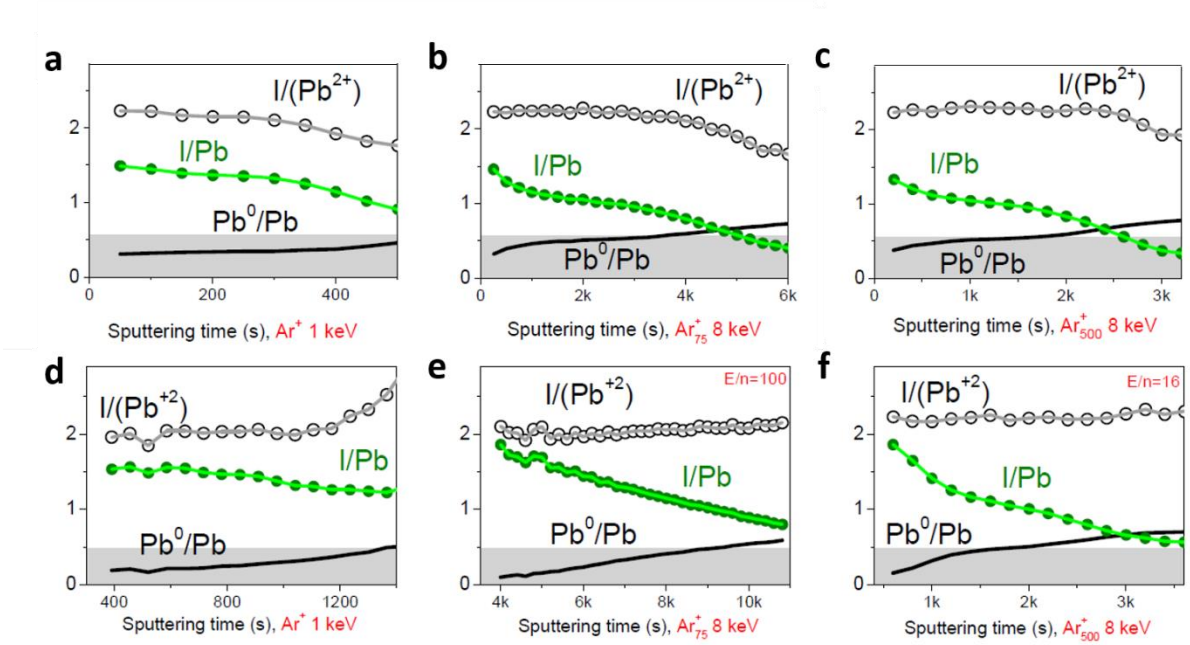

Figure 7. a), b) and c) Ratio evolutions of XPS depth profiles acquired on $MAPbI_3/TiO_2$ with monoatomic Ar^+ at 1 keV, Ar_{75}^+ clusters at 8 keV and Ar_{500}^+ 8 keV, respectively. d), e) and f) Ratio evolutions of XPS depth profiles acquired on Au/Spiro-MeOTAD/$MAPbI_3$/ TiO_2MAPbI_3/TiO_2 heterojunctions with monoatomic Ar^+ at 1 keV, Ar_{75}^+ clusters at 8 keV and Ar_{500}^+ 8 keV, respectively. Reproduced with permission.[173] Copyright 2019, Multidisciplinary Digital Publishing Institute.

3.5.2.Depth-resolved PES measurements

Another way to access the chemical information of HaPs in the sub-surface region or buried layers by PES is to increase the photon energy used for excitation by pursuing HAXPES measurements. Philippe *et al.*[174] performed a comparative study with two photon energies: 2100 and 4000 eV, (corresponding to ≈11 and ≈18 nm of probing depth, respectively) to compare the surface and quasi-bulk composition of four different perovskite compounds ($FAMAPbI_3$, $FAMACsPbI_3$, $FAMARbPbI_3$ and $FAMACsRbPbI_3$). The work presents a first attempt to retrieve the location of the different cations in the bulk. For double cation perovskites ($FAMAPbI_3$), they report an excess of PbI_2, located inside the bulk while unreacted precursor

(FAI) was still detected on the surface. By adding one or two A-site cations (Cs and/or Rb), the distribution of the iodine content then indicates a lower amount of PbI_2 inside the bulk. For triple cation perovskites ($FAMACsPbI_3$ and $FAMARbPbI_3$), Philippe *et al*. note two different trends regarding the localization of the additional cation species: the amount of Cs seems to be uniformly spread over the depths probed while Rb appears to be located deeper in the bulk. By adding a fourth cation inside the perovskite preparation ($FAMACsRbPbI_3$), a more homogenous distribution is observed over the probed bulk volume (Figure 8, a).

Jacobsson *et al*.[78] evaluated the influence of PbI_2 (excess, normal stoichiometry or deficiency) in $FA_{0.85}MA_{0.15}PbBr_{0.45}I_{2.55}$ films on SnO_2 substrates by HAXPES, in order to understand the chemical distribution. By performing compositional analysis at varied probing depths of ≈5, ≈11, and ≈15 nm (758 eV, 2100 eV and 4000 eV, respectively), they generate a coarse model that is consistent with a surplus of organic species (FAI) at the sample surface and unreacted PbI_2 located deeper inside the perovskite film (Figure 8, b). While an absolute quantification remains difficult, these depth-resolved compositions and related HAXPES experiments of HaP thin films yield a qualitative picture describing potential segregation processes in mixed HaPs.

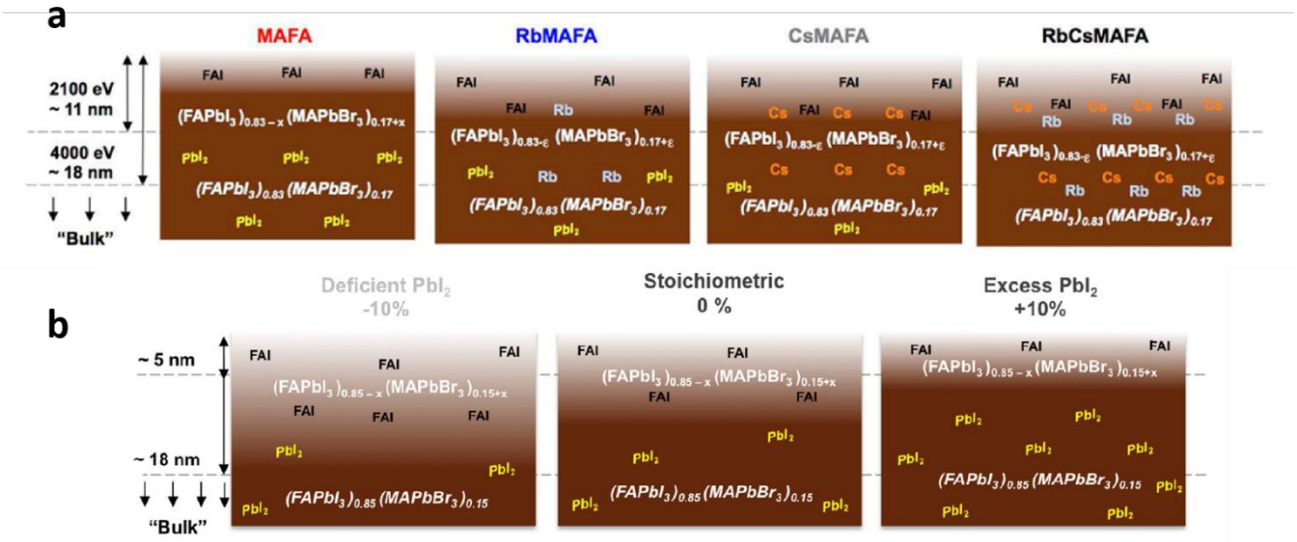

Figure 8. a) Schematic illustration summarizing the main differences observed by HAXPES between the perovskite materials containing two (MA/FA), three (Rb/MA/FA and

Cs/MA/FA), and four (Rb/Cs/MA/FA) cations. Reproduced with permission.[174] Copyright 2017, American Chemical Society. b) Schematic illustration summarizing the main difference observed by HAXPES between the perovskite materials with different stoichiometries of $MAPbI_3$ thin films (evaporated with a deficiency of PbI_2, a normal stoichiometry and an excess of PbI_2). Reproduced with permission.[78] Copyright 2016, American Chemical Society.

4. Specific challenges for the characterization of HaPs by PES methods

4.1.Stability and deviation from pristine surface conditions

4.1.1.Metallic lead formation during XPS measurements

A main issue observed during XPS measurement is the reduction of Pb^{2+} in the perovskite structure to elementary lead (Pb^0) as indicated in section 3.4.1.[175,176] Most strikingly, the occurrence of Pb^0 is not always observed in published reports, despite very similar set up of experimental conditions for measuring HaP films by XPS.[135,177] This apparent inconsistency raises questions about the degradation mechanism itself and the different means to minimize its evolution with beam damage effects during the measurement. Shkrob and Marin [178] used electron paramagnetic resonance spectroscopy to describe the tendency of the material to degrade into Pb^0. They suggest that Pb^0 clusters are generated through a radiolysis mechanism due to high energy X-rays. Different origins for the emergence of Pb^0 exist: the potential photolysis induced under visible light illumination (see also section 3.4.1)[147] and the film degradation due to intrinsic instability of HaP. To prevent the appearance of this measurement artifact as much as possible, so far only coarse guidelines had been proposed. For instance, McGettrick *et al.*[179] suggest to perform the analysis in less than 30 minutes and to keep samples in dark.

However, more recently, the systematic investigation of the dynamic and cause of this degradation process under XPS operating conditions has been pursued. Kerner *et al.*[151,152,180] showed that Pb^0 formation does not come from a simple PbI_2 photolysis, but more probably from the formation of Pb-N (*i.e.* lead amide formation). Furthermore, this reaction can be accelerated by the presence of a catalyst, e.g. a thin Au overlayer. In their experiment, this conclusion is evidenced by the stability of PbI_2 and even pristine $MAPbI_3$ films under X-ray irradiation, whereas the $MAPbI_3$ becomes unstable with the gold, which could catalyze the formation of metallic lead and is consistent with a Pb underpotential deposition process.

4.1.2.Modifications of surface stoichiometry and electronic properties

Impact of storage and measurements under UHV conditions

As laid out in section 2.1.2, PES measurements are usually performed in an ultra-high vacuum (UHV) environment. Due to the often hybrid nature of HaPs, this adds to the question about an evolution of the chemical composition during the PES measurements in vacuum. Indeed, the organic components are more volatile than the inorganic ones, leading to surface modification by a loss of the organic part, which then is also often accompanied by a loss of the more reactive halide species. Two studies [146,154] were conducted on $MAPbI_3$ films and its derivatives ($MAPbI_{3-x}Cl_x$ and $MAPbBr_{3-x}Cl_x$) showing the stability of these layers over 24 hours of measurements.

Das *et al.*[146] performed studies on UHV stability by monitoring potential changes in the XPS spectra of $MAPbI_3$ films every hour. They observed no modification in the chemical environment unless additional illumination is involved (Figure 9, a. and b., see also section 3.4.1). However, a slight decrease of the N and I content was detected due to the outgassing of residual MAI from the surface under vacuum and X-ray exposure. Xu *et al.*[154] corroborated

their results, with no modification in the chemical environment of $MaPbI_{3-x}Cl_x$ and $MAPbI_{3-x}Br_x$ after UHV storage.

In agreement with the observations by Das *et al.*,[146] a decrease of the I/Pb ratio has also been observed for $MAPbI_3$ films stored in vacuum for 50 h by Sun *et al.*[140] This change in composition was correlated with a large-scale homogenization of the surface composition and was suggested to result from a loss of MAI in UHV (Figure 9, c. and d.). Indeed, the N/Pb ratio similarly decreased irrespective of the $MAPbI_3$ films initial stoichiometry and the decrease in relative nitrogen content was accompanied by an increase of the ionization energy IE values.[181] This is in line with the observed variation of IE in $MAPbI_3$ films as a function of their stoichiometry, i.e. the MAI to PbI_2 ratio.[139] It is noteworthy that an increase of IE was also observed for $MAPbI_{3-x}Cl_x$ films stored overnight in UHV (10^{-9} mbar).[182] This change in IE corresponds to a work function WF increase upon UHV storage. Interestingly, the WF increase appeared to be reversible upon storage in high vacuum HV (10^{-6} mbar) with this reversal and thus WF decrease being associated with the effect of residual water vapor in HV as will be explained in more detail below. Therefore, the effects of the low-pressure conditions on the electronic properties seem to depend also on the pressure range involved.

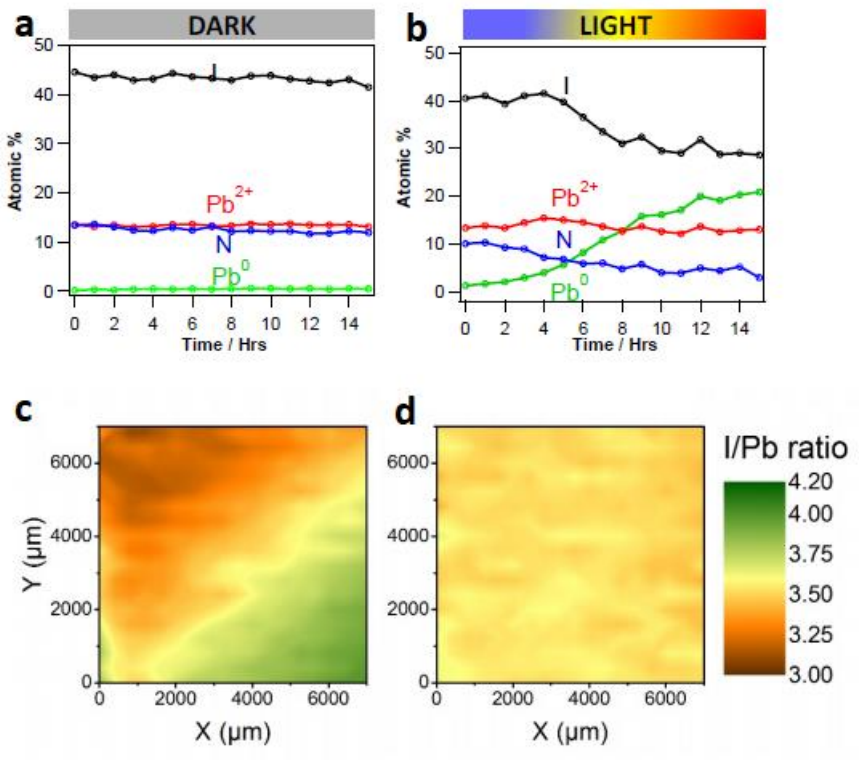

Figure 9. a) and b) Evolution over time of the relative elemental concentration of a $MAPbI_3$ film measured by XPS in UHV, in dark and under additional illumination, respectively. Reproduced with permission.[146] Copyright 2018, Royal Society of Chemistry. c) and d) Maps of I/Pb ratio of $MAPbI_3$ films after storage in N_2-filled glovebox and vacuum for 50h, respectively. Reproduced with permission.[140] Copyright 2018, American Chemical Society.

Impact of exposure to H_2O

Liquid water can drive the conversion of $MAPbI_3$ perovskite films into PbI_2.[9,183] In environments relevant for perovskite films and devices during their application or characterization, the partial pressure of water ranges from $<10^{-6}$ mbar, as in inert gas glove boxes or in HV conditions, to several mbar, as in ambient air. The investigation of the impact of water at these partial pressures is highly relevant in order to understand the potential impact of water on the optoelectronic and structural properties of perovskites and their eventual degradation mechanism and in consequence will have an effect on any PES analysis.[184–186]

Exposure to low water partial pressure of 10^{-6} mbar readily induces a work function decrease for $MAPbI_{3-x}Cl_x$ films; the phenomenon is reversible upon storage in UHV or by mild heating.[182] This work function change is attributed to the water dipole moment at the perovskite surface. Exposure to higher water content of 4 mbar (17 % RH at 20°C) led not only to a work function decrease but also to a concomitant shift of the VBM by 0.3 eV to higher binding energy, indicating that the sample appears to be more n-type (Figure 10). Similar trends in the XPS core levels were also observed for halide perovskite films prepared by thermal evaporation.[187] The pronounced shift of E_F in the band gap can correspond to the increase of the density of defect states with higher water doses, possibly related to an increase of the Pb^0 content. Indeed, generation of Pb^0 upon exposure to 9 mbar water partial pressure (30% RH at 25 °C) has been detected from NAP-XPS studies on thermally evaporated perovskite films.[32] Those studies highlight the impact of variation in the water content of the environment on the electronic properties of the HaPs. This is especially crucial, since perovskite devices are at times unintentionally prepared under varying relative humidity conditions. It is however important to keep in mind that the modifications observed on surfaces can also be induced by the presence of contaminants when samples are exposed to atmosphere and different environmental conditions. Specific attention needs to be paid on the experimental conditions to account for contaminant-dependent charging effects. Thus, the comparison/coupling of PES studies with complementary techniques can be helpful.

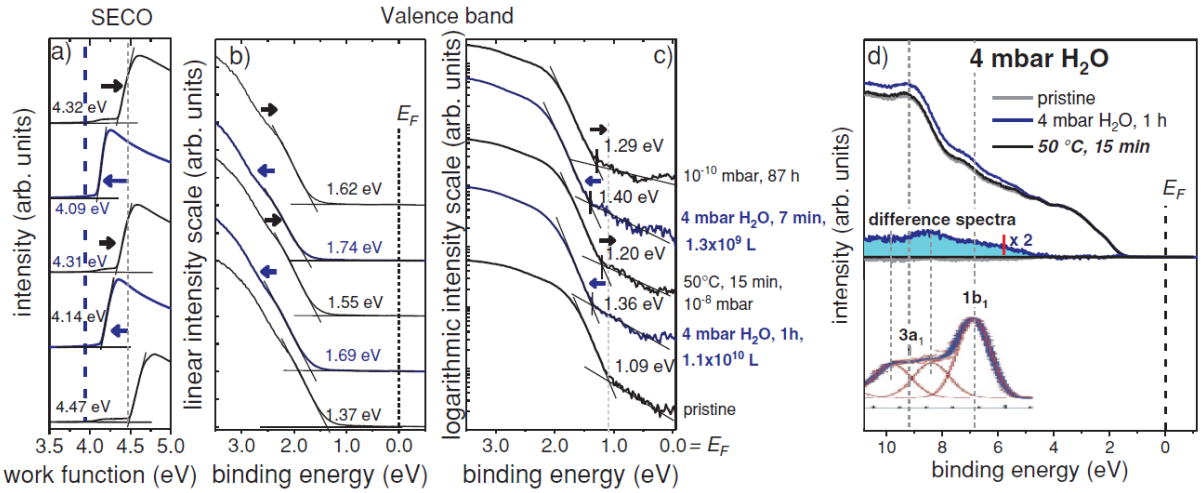

Figure 10. a) SECO, and valence band spectra plotted on b) a linear and c) logarithmic intensity scale of $MAPbI_{3-x}Cl_x$ films exposed to 4 mbar water partial pressure, followed by UHV storage or mild heating. d) Wide range valence band spectra from b) and corresponding difference spectra exhibiting features similar to those of liquid water (bottom inset). Reproduced with permission.[182] Copyright 2018, Wiley.

Impact of exposure to O_2

In addition to water, perovskite films in ambient conditions are primarily exposed to oxygen. Perovskite samples transferred from a N_2-glove box to vacuum conditions without initial exposure to air exhibited a parallel increase of the work function and shift of the VBM to higher binding energy upon exposure to 50 mbar O_2. Thus, in contrast to water, oxygen leads to the shift of E_F towards the mid-gap position, i.e. apparently the n-type doping of the pristine $MAPbI_{3-x}Cl_x$ perovskite surface is diminished.[182,187] This can suggest the oxidation of Pb^0 defects at the film surface as observed in the case of $MAPbBr_3$ films.[188] The trend in the energy level shift also indicates that oxygen acts as an acceptor, which can readily capture an electron and convert into superoxide (O_2^-) upon photoexcitation. The latter can then initiate degradation of the $MAPbI_3$ film by the deprotonation of the MA cation,[189] which is then released from the film surface, and the subsequent formation of PbI_2. Noteworthy, as-prepared perovskite

samples, which were exposed to air exhibited a shift of the energy levels similar to that observed upon exposure to pure oxygen only.[182] The shift is translated into an increase of the WF and a shift of the VBM to lower binding energy by up to 0.6 eV after an exposure time as short as 15 min.[139,182] Therefore, with regard to the electronic properties, the effect of oxygen prevails over the effect due to water in ambient air, which is likely related to the substantially higher oxygen partial pressure in air in comparison to the corresponding partial pressure of water.

These combined observations stress the impact of environmental gasses the HaPs can be exposed to on the electronic properties of their surfaces. Furthermore, they emphasize the importance of controlling the environment conditions in order to reliably assess and compare PES results.

4.2.Band edge determination

Initially, the determination of the band edge positions proved to be an ambitious endeavor for HaP films, as a precise discrimination between bulk, surface or defect states from PES data remains a challenge. This is of course true for all materials that exhibit a high degree of structural disorder and/or high defect densities.

A first approach for band edge determination via PES was given by Kraut *et al.*, who offered an approximation of E_{VBM} at a semiconductor surface by performing a linear regression to the leading edge of the valence band region in the XPS spectra of crystalline Ge(110) and GaAs(110) surfaces. The results were in good agreement with onsets determined from theoretical calculations of the valence band DOS used as reference for these pristine surfaces.[190] This fitting procedure was subsequently adopted for a range of semiconductor systems, and worked particularly well for conjugated organic semiconductor samples, for which the frontier molecular orbitals often constitute the delocalized π electron system.[191] However, this approximation can be erroneous for semiconductors that do not exhibit sharp energy level

onsets, as is on the one hand the case for materials that exhibit a significant contribution of tail states. HaPs, on the other hand, exhibit a particularly low DOS at the band edges, that becomes hard to observe in a standard PES experiment.[109]

Now, the extrapolation of the perceived linear section of the band onset can become arbitrary and lead to VBM positions that are too deep, which would yield unphysical results such as band gap values that were too large. Similar observations were made for PbS-based semiconductor systems, which share the lead component with a significant sub-set of the technologically relevant lead-based HaPs, where a linear extrapolation of the band edge would have resulted in unrealistically large band gaps.[192]

To visualize the contribution of the low DOS at the valence band edge and for a first approximation of E_{VBM}, the spectra can be plotted on a semi-logarithmic scale. This has been done for several HaPs recently and even before for several organic semiconductors,[193] and was pursued by Schulz *et al.* for the estimation of the E_{VBM} in methylammonium lead halide perovskites for the first time. [98]

In a combined theoretical and experimental study, Endres *et al.* employed PES/IPES to determine both, valence band maximum and conduction band minimum, of $MAPbI_3$, $MAPbBr_3$ and $CsPbBr_3$ thin films.[109] In Figure 11 a and b, we show the measured UPS and IPES valence and conduction band spectra of $MAPbI_3$, which were used to fit DFT calculations including spin orbit coupling. The calculated spectra are appropriately shifted and scaled to achieve a good alignment of the spectral features over a broad energy range. From this fit, Endres accurately determined the band onsets of the $MAPbI_3$ thin film, deposited on top of a TiO_2 electron transport layer, resulting in an IE of 5.2 eV and an EA of 3.6 eV. Here, plotting the spectra on a semi-logarithmic scale aids in visualizing the transport gap between valence and conduction band. The scenario of a low DOS has been hypothesized for $MAPbI_3$, for which

DFT calculations point to a strong coupling between the anti-bonding orbitals (primarily Pb 6s and I 5p), with only a small contribution to the DOS at the R-point in reciprocal space.[194] We note that this small contribution to the DOS, and hence "soft" band edge, is already hardly observable in the presented angle-integrated PES experiments. Angle-resolved photoemission spectroscopy (ARPES) experiments could be explicitly "blind" to this direction of the band progression due to the chosen crystal orientation and measurement geometry. Thus, initial ARPES measurements of $MAPbI_3$ single crystals by Lee *et al.* did not reveal this intricacy of the HaP electronic structure, not excluding secondary effects such as potential beam damage, surface impurities or a mixed tetragonal-cubic structural order to the specific sample.[195]

Zu and coworkers further investigated the valence band determination of polycrystalline $MAPbI_3$ and $MAPbBr_3$ single crystal and thin film samples by ARPES under excitation by a lab-based UV source, contrasting the synchrotron-based study presented by Lee *et al.* presented in the previous paragraph.[106] The maximum of the EDC as measured by PES is plotted for individual values of the k-vector along the M-X-R direction in reciprocal space in Figure 11 c. The data includes values from the EDC onset determination for a fitting procedure on a linear and logarithmic scale and shows that on a linear scale the range of onset values with respect to E_F spans from 1.4 eV to over 1.9 eV. In comparison, the logarithmic evaluation yields onset values with a smaller spread ranging between 1.3 eV and 1.4 eV below E_F. The implications are well captured in the corresponding angle-integrated data that correspond to simulated UPS spectra, shown, again, on a linear and a logarithmic scale in Figure 11 d. While the linear fit to the leading edge would lead to an erroneously deep VBM, exceeding the transport gap, a realistic value of 1.4 eV with respect to E_F is obtained from the logarithmic representation.

Thus, while the mathematical treatment is not as straightforward, the logarithmic representation offers a more reliable determination of E_{VBM}. This is true even for polycrystalline perovskite thin films, which should in principle exhibit all crystal orientations - and hence lead to an

integration over the entire Brillouin zone - but often exhibit a high degree of texture in reality. As a consequence, part of the signal originating from the DOS at the edge of the Brillouin zone might be suppressed. Zu *et al.* validate their approach for polycrystalline thin film samples and obtain UPS spectra that match well to the previously simulated spectra from the single crystal sample.[106]

As a closing remark to this section we note that the treatment of the background becomes slightly arbitrary in the logarithmic plot. In the study by Zu, the robustness of the approach was tested for various levels of background noise leading to consistent results. Ideally, the experiment is pursued by using monochromatic UV radiation as excitation, otherwise the subtraction of the contributions of inevitable satellite lines, despite being a possible data treatment procedure if pursued with great care, increases the ambiguity of the fit to the background level.

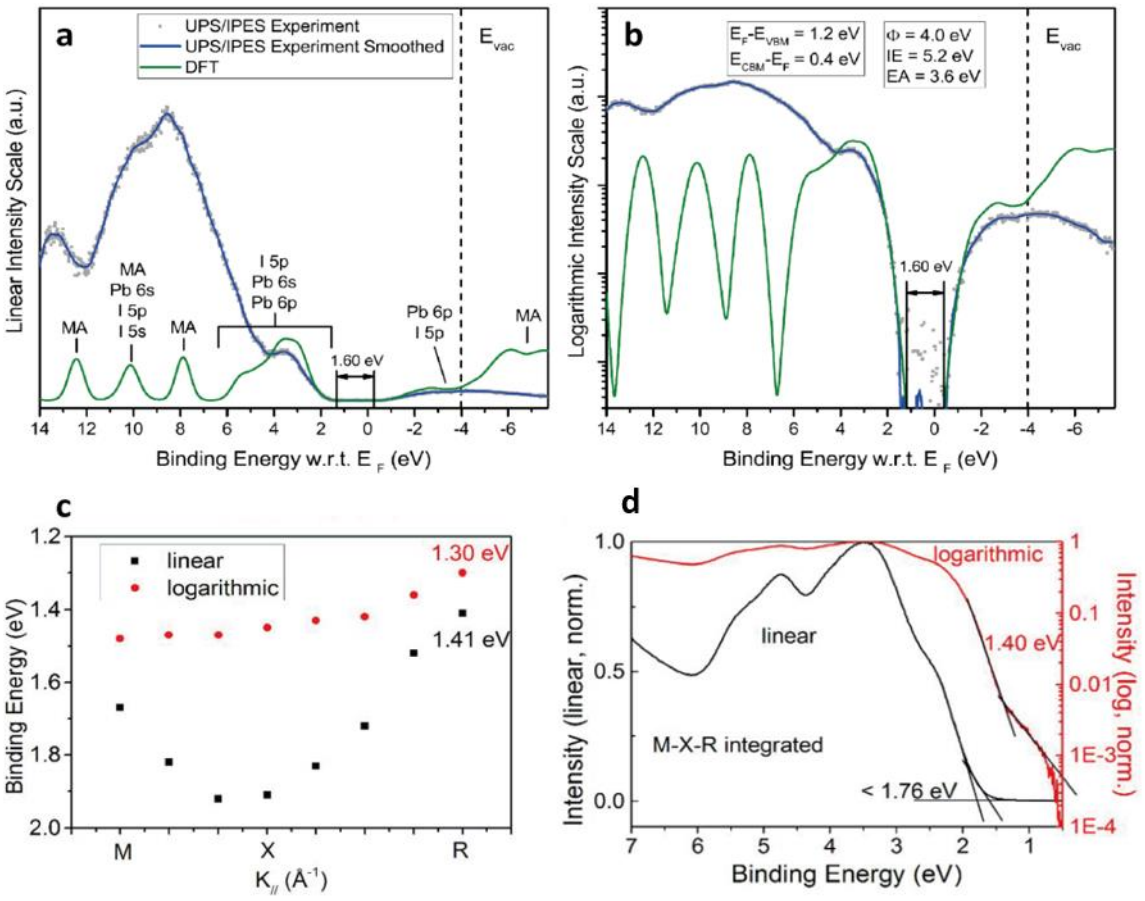

Figure 11. Band edge determination. a) and b) Comparison between measured UPS and IPES spectra for an approximately 300 nm thick $MAPbI_3$ film on TiO_2, and DFT-calculated spectra. The energy scale is referenced to $E_F = 0$ and the intensity is plotted on a linear and logarithmic scale, respectively. Major atomic orbital contributions are indicated in the spectra, while values for IE, EA and the energy gap were extracted from the measured and fitted band onsets in conjunction with the read-out of the work function WF from the secondary electron cut-off in the UPS measurements (not shown here). Reproduced with permission.[109] Copyright 2016, American Chemical Society. c) Valence band maximum determination from the EDCs of UPS data from a $MAPbI_3$ single crystal, using linear and logarithmic intensity scales for selected *k* values along the M-X-R direction. d) Simulated UPS spectrum for a polycrystalline $MAPbI_3$, obtained by summation of a set of measured EDCs plotted on linear and logarithmic scales. Reproduced with permission.[106] Copyright 2019, American Chemical Society.

4.3.Fermi level pinning and surface states

We finally turn to a set of very specific observations that were made for PES data on HaP semiconductors, i.e. the measured position of the Fermi level in the gap. As indicated already in the introduction, the offset between energy levels at an interface is a key parameter for electronic transport process across the interface. Particularly, in perovskite solar cells, a mismatch between the transport levels of the carrier extraction layer and the perovskite film could limit the device parameters such as open circuit voltage (Voc) or introduce an energy barrier that impedes carrier extraction, and could as well degrade the carrier selectivity by allowing carrier cross-over and recombination.

In first approximation, this offset can be derived from – or at least be informed by – the position of the corresponding band onsets, i.e. the distance of the band extremum from E_F, of the individual layers forming the interface. Hence, the measurement of the valence band and

conduction band onsets by PES (and IPES, respectively) becomes of paramount importance. In HaPs, we find the position of the valence band onset as determined by PES to be dependent on the substrate underneath, even though this interface is located several hundreds of nanometers below the probed HaP surface as introduced in section 3.3.2.

Specifically, we find that the choice of the bottom oxide transport layer as a substrate would drastically change E_F within the perovskite film on top.[10,101] The exact evolution of E_F throughout the bulk of the HaP layer including potential band bending has not been directly observed yet. A corresponding summary of the energetic alignment in conventional and inverted perovskite solar cells as estimated by PES/IPES measurements is depicted in Figure 12 b. Note that the band offset at the oxide charge transport layer and perovskite remains an educated guess as the position of E_F in the perovskite layer has only been determined for the top surface layer whereas no direct information for the interface deeply buried underneath has been obtained.

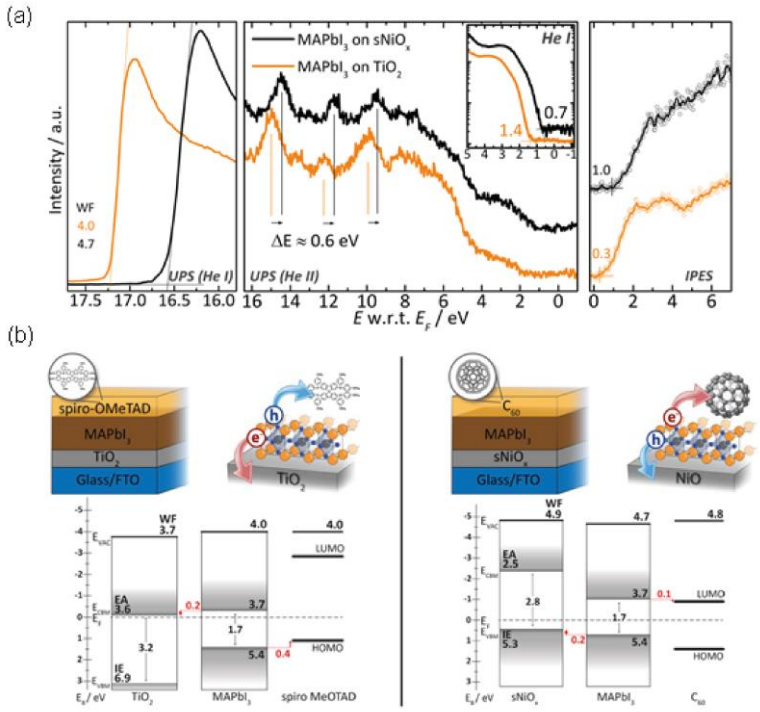

Figure 12. a) Comparison of the Fermi level position in $MAPbI_3$ thin-films on different substrates by PES/IPES. Reproduced with permission.[10] Copyright 2015, Wiley. b) Energy

level diagram of $MAPbI_3$ adjacent to different charge transport layers. Reproduced with permission.[19] Copyright 2018, American Chemical Society.

To date, the root cause for this tractability of E_F in the band gap for HaP films remains elusive. To further explain the phenomenon a closer look at potential surface states of the perovskite film and at the saturation of such states is warranted. A targeted approach to evaluate the effect of surface states on the HaP semiconductor and of trap state densities on the energy level alignment with adjacent organic charge transport layers was pursued by Zu *et al.*[196]

In this context, we point to a separate study, in which the formation of substantial amounts of metallic lead was found in $MAPbI_{3-x}Cl_x$ samples, when those were illuminated in the vacuum chamber.[147] This treatment can thus be used to precondition the $MAPbI_3$ surface as pristine, i.e. MAI-terminated, or highly defective after illumination, i.e. enriched with Pb^0. Note that the $MAPbI_{3-x}Cl_x$ film in this particular case was produced on an organic semiconductor film (PEDOT:PSS), which presumably leads to a mid-gap position of E_F. However, now the light-induced formation of Pb^0-related donor states in the upper part of the gap pins the Fermi level close to the CBM at the surface, leading to a downward band bending, as depicted in Figure 13. In the following, the surfaces are hence denoted as low density of state surfaces (low DoSS) corresponding to the pristine MAI-terminated sample with a minimal amount of Pb^0 donor states, or high density of states surfaces (high DoSS), for the *in-vacuo* illuminated sample, respectively. Subsequently, Zu *et al.* deposited the acceptor molecule HAT-CN in incremental steps and tracked the energy level alignment by PES. Upon formation of the first very thin (4 Å) overlayer of HAT-CN on top of the $MAPbI_{3-x}Cl_x$ sample, the core levels of the HaP compound shift to lower binding energy, which corresponds to a shift of E_F from close to the CBM to a mid-gap position at the HaP/Hat-CN interface. In this low DoSS case, the HAT-CN

acceptor molecules compensate the donor states, effectively unpinning the Fermi level and restoring the flat-band condition.

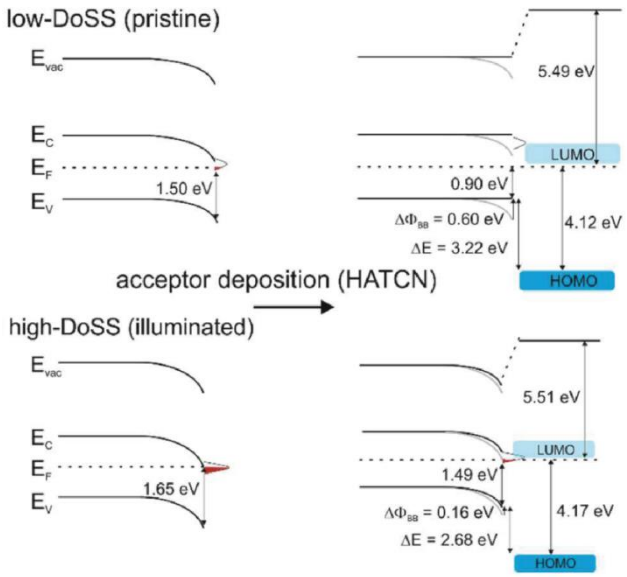

Figure 13. Interfacial energy level diagrams, derived from the PES data for pristine (low-DoSS) and defective (high-DoSS) $MAPbI_{3-x}Cl_x$ samples, without (left) and with (right) HAT-CN overlayer on top. Reproduced with permission.[196] Copyright 2017, American Chemical Society.

We make a different observation for the high-DoSS surface. Here, the amount of Pb^0 compared to Pb^{2+} as seen by XPS measurements is decreased with increasing HAT-CN film thickness, indicating that the reduced Pb is re-oxidized, while the shift of the Pb^{2+} core level is minimal, which means that not all donor states are compensated on the HaP side of the interface. Consequently, E_F, remains pinned to the CBM. The two cases are summarized in the energy level diagrams in Figure 13. The PES analysis of this doped HaP interface reveals, that for an initial low-DoSS HaP surface a strong organic acceptor molecule can induce upward band bending which results from the saturation of donor like defects, while a high-DoSS HaP surface maintains its n-type character as E_F is pinned to the CBM.

While this case exemplifies how PES is a powerful tool to analyze defect states at HaP surfaces and even link these defects to oxidation states of the chemical components in the HaP structure, we note that complementary techniques are required to complete the picture and characterize the interface under different conditions. For example, optical probes can help to assess recombination and hence the electronic activity of (surface/interface) defects, whereas dark contactless probe microscopy methods, i.e. scanning tunneling spectroscopy (STS) or Kelvin probe force microscopy (KPFM), yield additional information on the surface electronic properties, such as Fermi level pinning and band bending.[197]

5.Conclusion and outlook

Throughout this review, our central focus is on the possibilities and intricacies in the use of PES techniques for research on HaP materials. We highlight the approach to couple complementary PES techniques, such as UPS/IPES/XPS, to obtain an accurate description of the chemical and electronical properties of HaP surfaces.

5.1.Good practices for PES measurements and data treatment for HaPs

In a previous article, Hoye *et al.*[47] gave a first overview on good practices for the analysis and characterization of HaP samples including a section on precautions necessary to perform PES measurements. Here, we expand on this notion and highlight the intricacies for the extraction of reliable data from PES measurements of HaP materials. As a general striking result of this analysis we may state that the data and results obtained can exhibit significant variance depending strongly on sample preconditioning and, equally important, measurement conditions. While, we usually try to avoid transient behavior during the measurement, we also

note that carefully tracking changes of the sample chemical properties bears the potential to unravel critical chemical processes in the HaP such as degradation and phase segregation.

As a first point, we underline that detailed knowledge of the full sample stack (substrates, architecture, type of HTL and ETL layers…), as well as the growth conditions of the HaP film are keys for the interpretation of the PES data. Indeed, the recently published literature shows that the large range of reported values is strongly dependent on these, sometimes seemingly secondary, parameters. This could lead to possibly erroneous interpretation of the findings, especially with respect to the electronic properties and surface energetics (e.g the WF) of the HaP films. In addition, compositional inhomogeneities of the HaP layers can also affect these parameters and need to be carefully tracked as well.

Then, we report on the role of extrinsic factors on the PES results. As a primary concern we note that while pristine HaP films can be found to be stable under adapted measurement conditions and often exhibit non-reactive surface termination, i.e. a closed-shell electron system of the organic component, the sample history can significantly affect the PES results, particularly when the HaP films have been exposed to air, with different humidity levels and under illumination.

In this scope, we highlight that HaP films can, in fact, exhibit strong chemical reaction, before and during the PES experiment. For instance, the choice of the contact layer proved to be critical and could exhibit catalytic behavior. Another important point in this regard is the inherent degradation of HaPs materials under X-rays exposure, thus, during the PES spectra acquisition. This exposure can be responsible for apparent changes in the chemical composition and thereby impede a quantitative analysis, as well as the accurate identification of the electronic properties. Such artifacts can however be avoided, by reducing the source intensity while at the same time recording data over several locations on a homogenous HaP surface, limiting thus the exposure time in one spot and the overall radiation dose.

Finally, while PES/IPES methods are potent tools for the determination of key electronic properties such as the band onsets and the Fermi level position in the band gap, specific challenges concern the data acquisition and treatment for HaP samples. Among these challenges is the precise fitting of the band edge which is an intricate task due to the soft energy onsets related to the low DOS at the band edge for several HaP compounds. In this case, good practice is to apply theoretical modelling and coupling the experimental values to DFT calculations, but also to corroborate the findings by STS or KPFM. Indeed, a combination of these measurements has been applied in the past years to catalog the energy level positions in HaP with increasing success. Note, that in this context Fermi level pinning to defect states, resulting from the measurement conditions, can alter the state of the pristine HaP surface. Thus, despite all the good practices, inherent changes to the HaP surface can occur in the measurement process.

5.2.Outlook

While the observed transient behavior of the HaP surface during the PES experiment complicates standardized data evaluation, it also offers one of the most compelling perspectives for future dedicated PES studies. More precisely, we refer to the pursuit of PES measurements in an *operando* mode. Here, the term is associated to minutely controlled measurement conditions and complementary experiments that are performed in parallel to the PES analysis in the same experimental sequence.

Here, we refer to *operando* XPS in terms of surface characterization modulated by electrical and/or light bias. The important predicament is that we capture the most relevant physical properties (work function, defect density, etc.) and chemical properties (stoichiometry, oxidation states, etc.) at time scales compatible with the chemical processes that are associated with ion migration or desorption.

This approach thus constitutes a combination of advanced optical and electron spectroscopies and microscopies, to correlate charge carrier dynamics with the interface energetics and species formation. The focus of this endeavor should be on a precise measurement of interface energetics, energy barriers, and associated charge carrier dynamics (transfer and recombination rates). While doing so, we need to keep in mind that, due to the metastability of HaP compound, the measurement probes and parameters (light, bias, etc.) can cause chemical and structural reorganization, which needs to be taken into consideration for the data interpretation.

Finally, these findings would reveal potential precursors at the interface between HaPs and adjacent functional layer and allow us to track such chemical precursors under less invasive measurement conditions (lowered flux) in the PES experiment. As a final remark, we note that among these different strategies, measurements in a NAP-PES configuration further targets the quantification of the sample reactivity with extrinsic species such as environmental gases as a next decisive step to investigate HaP stability.

6.Acknowledgements

P.S. and M.R. thank the French Agence Nationale de la Recherche for funding under the contract ANR-17-MPGA-0012.

Received: ((will be filled in by the editorial staff))
Revised: ((will be filled in by the editorial staff))
Published online: ((will be filled in by the editorial staff))

7.References

[1] D. B. Mitzi, S. Wang, C. a Feild, C. a Chess, a M. Guloy, *Science (80-.).* **1995**, *267*, 1473.

[2] D. A. Egger, A. Bera, D. Cahen, G. Hodes, T. Kirchartz, L. Kronik, R. Lovrincic, A. M. Rappe, D. R. Reichman, O. Yaffe, *Adv. Mater.* **2018**, *30*, 1800691.

[3] C. R. Kagan, *Science (80-.).* **1999**, *286*, 945.

[4] A. Kojima, K. Teshima, Y. Shirai, T. Miyasaka, *J. Am. Chem. Soc.* **2009**, *131*, 6050.

[5] Y. C. Kim, K. H. Kim, D.-Y. Son, D.-N. Jeong, J.-Y. Seo, Y. S. Choi, I. T. Han, S. Y. Lee, N.-G. Park, *Nature* **2017**, *550*, 87.

[6] P. Schulz, D. Cahen, A. Kahn, *Chem. Rev.* **2019**, *119*, 3349.

[7] D. J. O'Connor, B. A. Sexton, R. S. C. Smart, Eds. , *Surface Analysis Methods in Materials Science*, Springer Berlin Heidelberg, Berlin, Heidelberg, **1992**.

[8] K. X. Steirer, P. Schulz, G. Teeter, V. Stevanovic, M. Yang, K. Zhu, J. J. Berry, *ACS Energy Lett.* **2016**, *1*, 360.

[9] B. Philippe, B. W. Park, R. Lindblad, J. Oscarsson, S. Ahmadi, E. M. J. Johansson, H. Rensmo, *Chem. Mater.* **2015**, *27*, 1720.

[10] P. Schulz, L. L. Whittaker-Brooks, B. A. MacLeod, D. C. Olson, Y.-L. Loo, A. Kahn, *Adv. Mater. Interfaces* **2015**, *2*, 1400532.

[11] N. F. Mott, *Math. Proc. Cambridge Philos. Soc.* **1938**, *34*, 568.

[12] R. L. Anderson, *IBM J. Res. Dev.* **1960**, *4*, 283.

[13] C. Tejedor, F. Flores, *J. Phys. C Solid State Phys.* **1977**, *11*, L19.

[14] X. Crispin, V. Geskin, A. Crispin, J. Cornil, R. Lazzaroni, W. R. Salaneck, J.-L. Brédas, *J. Am. Chem. Soc.* **2002**, *124*, 8131.

[15] M. Oehzelt, N. Koch, G. Heimel, *Nat. Commun.* **2014**, *5*, 4174.

[16] J. Hwang, A. Wan, A. Kahn, *Mater. Sci. Eng. R Reports* **2009**, *64*, 1.

[17] A. Fakharuddin, L. Schmidt-Mende, G. Garcia-Belmonte, R. Jose, I. Mora-Sero, *Adv. Energy Mater.* **2017**, *7*, 1700623.

[18] A.-N. Cho, N.-G. Park, *ChemSusChem* **2017**, *10*, 3687.

[19] P. Schulz, *ACS Energy Lett.* **2018**, *3*, 1287.

[20] L. Qiu, S. He, L. K. Ono, Y. Qi, *Adv. Energy Mater.* **2019**, 1902726.

[21] H. Hertz, *Ann. der Phys. und Chemie* **1887**, *267*, 983.

[22] A. Einstein, *Ann. Phys.* **1905**, *322*, 132.

[23] D. Briggs, M. P. Seah, *Practical Surface Analysis by Auger and X-Ray Photoelectron Spectroscopy*, John Wiley And Sons Ltd, Chichester, UK, **1984**.

[24] M. P. Seah, *Surf. Sci.* **1999**, *420*, 285.

[25] J. E. Castle, A. M. Salvi, *J. Vac. Sci. Technol. A Vacuum, Surfaces, Film.* **2001**, *19*, 1170.

[26] J. Végh, *J. Electron Spectros. Relat. Phenomena* **2006**, *151*, 159.

[27] S. Hüfner, *Photoelectron Spectroscopy*, Springer Berlin Heidelberg, Berlin, Heidelberg, **2003**.

[28] S. Hüfner, *Very High Resolution Photoelectron Spectroscopy*, Springer Berlin Heidelberg, Berlin Heidelberg, **2007**.

[29] J. F. Watts, J. Wolstenholme, *An Introduction to Surface Analysis by XPS and AES*, John Wiley & Sons, Ltd, Chichester, UK, **2003**.

[30] D. J. O'Connor, B. A. Sexton, R. S. C. Smart, Eds. , *Surface Analysis Methods in Materials Science*, Springer Berlin Heidelberg, Berlin, Heidelberg, **2003**.

[31] A. Jürgensen, N. Esser, R. Hergenröder, *Surf. Interface Anal.* **2012**, *44*, 1100.

[32] J. Chun-Ren Ke, A. S. Walton, D. J. Lewis, A. Tedstone, P. O'Brien, A. G. Thomas, W. R. Flavell, *Chem. Commun.* **2017**, *53*, 5231.

[33] Chen, Solanki, Pan, Sum, *Coatings* **2019**, *9*, 535.

[34] P. Van Der Heide, *X-Ray Photoelectron Spectroscopy: An Introduction to Principles and Practices*, Wiley, Hoboken, NJ, **2011**.

[35] M.P.Seah, W.A.Dench, *Surf. Interface Anal.* **1979**, *1*, 2.

[36] S. Tanuma, C. J. Powell, D. R. Penn, *J. Vac. Sci. Technol. A Vacuum, Surfaces, Film.* **1990**, *8*, 2213.

[37] B. Feuerbacher, B. Fitton, R. F. Willis, Eds. , *Photoemission and the Electronic Properties of Surfaces*, John Wiley & Sons, New York, **1978**.

[38] B. Philippe, G. J. Man, H. Rensmo, in *Charact. Tech. Perovskite Sol. Cell Mater.*, Elsevier, **2020**, pp. 109–137.

[39] S. Tanuma, C. J. Powell, D. R. Penn, *Surf. Interface Anal.* **1994**, *21*, 165.

[40] C. J. Powell, A. Jablonski, *Nucl. Instruments Methods Phys. Res. Sect. A Accel. Spectrometers, Detect. Assoc. Equip.* **2009**, *601*, 54.

[41] S. Tougaard, *J. Electron Spectros. Relat. Phenomena* **2010**, *178–179*, 128.

[42] W. S. M. Werner, W. Smekal, C. J. Powell, *NIST Database for the Simulation of Electron Spectra for Surface Analysis (SESSA). v 2.1.1*, **2019**.

[43] S. Tougaard, F. Yubero, *QUEELS - XPS: Software for Quantitative Analysis of Electron Energy Loss in XPS Spectra. v 2.1*, **2011**.

[44] S. Tougaard, *QUASES: Software for Qunatitative XPS/AES of Surface Nanostructures by Analysis of the Peak-Shape and the Background. v 7.01*, **2016**.

[45] W. S. M. Werner, W. Smekal, T. Hisch, J. Himmelsbach, C. J. Powell, *J. Electron Spectros. Relat. Phenomena* **2013**, *190*, 137.

[46] S. Tougaard, *J. Vac. Sci. Technol. A Vacuum, Surfaces, Film.* **1996**, *14*, 1415.

[47] R. L. Z. Hoye, P. Schulz, L. T. Schelhas, A. M. Holder, K. H. Stone, J. D. Perkins, D. Vigil-Fowler, S. Siol, D. O. Scanlon, A. Zakutayev, A. Walsh, I. C. Smith, B. C. Melot, R. C. Kurchin, Y. Wang, J. Shi, F. C. Marques, J. J. Berry, W. Tumas, S. Lany, V. Stevanović, M. F. Toney, T. Buonassisi, *Chem. Mater.* **2017**, *29*, 1964.

[48] S. Morton, in *Handb. Spectrosc.*, Wiley-VCH Verlag GmbH & Co. KGaA, Weinheim, Germany, **2014**, pp. 779–820.

[49] J. F. Moulder, W. F. Stickle, P. E. Sobol, K. D. Bomben, *Handbook of X-Ray Photoelectron Spectroscopy*, **1992**.

[50] A. J. Roberts, C. E. Moffitt, *J. Electron Spectros. Relat. Phenomena* **2019**, *231*, 68.

[51] C. S. Fadley, in *Hard X-Ray Photoelectron Spectrosc.* (Ed.: J. Woicik), Springer International Publishing, Cham, **2016**.

[52] J. C. Woicik, Ed. , *Hard X-Ray Photoelectron Spectroscopy (HAXPES)*, Springer International Publishing, **2016**.

[53] T. J. Jacobsson, S. Svanström, V. Andrei, J. P. H. Rivett, N. Kornienko, B. Philippe, U. B. Cappel, H. Rensmo, F. Deschler, G. Boschloo, *J. Phys. Chem. C* **2018**, *122*, 13548.

[54] N. V Smith, *Reports Prog. Phys.* **1988**, *51*, 1227.

[55] C. G. H. Walker, in *Handb. Spectrosc.*, Wiley-VCH Verlag GmbH & Co. KGaA, Weinheim, Germany, **2014**, pp. 709–740.

[56] A.-M. Gonçalves, M. Bouttemy, O. El Ali, A. Eb, C. Mathieu, J. Vigneron, A. Etcheberry, R. White, P. Mack, *Surf. Interface Anal.* **2010**, *42*, 775.

[57] A. X. Gray, in *Hard X-Ray Photoelectron Spectrosc.* (Ed.: J. Woicik), Springer International Publishing, **2016**, pp. 141–157.

[58] M. R. Linford, V. S. Smentkowski, J. T. Grant, C. R. Brundle, P. M. A. Sherwood, M. C. Biesinger, J. Terry, K. Artyushkova, A. Herrera-Gómez, S. Tougaard, W. Skinner, J.-J. Pireaux, C. F. McConville, C. D. Easton, T. R. Gengenbach, G. H. Major, P. Dietrich, A. Thissen, M. Engelhard, C. J. Powell, K. J. Gaskell, D. R. Baer, *Microsc. Microanal.* **2020**, 1.

[59] ASTM international E1523-09, *Standard Guide to Charge Control and Charge Referencing Techniques in X-Ray Photoelectron Spectroscopy*, **2009**.

[60] ASTM international E1078-14, *Standard Guide for Specimen Preparation and Mounting in Surface Analysis*, **2014**.

[61] ASTM international E1829-14, *Standard Guide for Handling Specimens Prior to Surface Analysis*, **2014**.

[62] ASTM international E2108-16, *Standard Practice for Calibration of the Electron Binding-Energy Scale of an X-Ray Photoelectron Spectrometer*, **2016**.

[63] ISO standard 18554, *Surface Chemical Analysis — Electron Spectroscopies — Procedures for Identifying, Estimating and Correcting for Unintended Degradation by X-Rays in a Material Undergoing Analysis by X-Ray Photoelectron Spectroscopy*, **2016**.

[64] ISO standard 19318, *Urface Chemical Analysis — X-Ray Photoelectron Spectroscopy — Reporting of Methods Used for Charge Control and Charge Correction*, **2004**.

[65] ISO standard 20579-4, *Surface Chemical Analysis — Guidelines to Sample Handling, Preparation and Mounting — Part 4: Reporting Information Related to the History, Preparation, Handling and Mounting of Nano-Objects Prior to Surface Analysis*, **2018**.

[66] D. R. Baer, K. Artyushkova, C. Richard Brundle, J. E. Castle, M. H. Engelhard, K. J. Gaskell, J. T. Grant, R. T. Haasch, M. R. Linford, C. J. Powell, A. G. Shard, P. M. A. Sherwood, V. S. Smentkowski, *J. Vac. Sci. Technol. A* **2019**, *37*, 031401.

[67] S. Béchu, A. Loubat, M. Bouttemy, J. Vigneron, J.-L. Gentner, A. Etcheberry, *Thin Solid Films* **2019**, *669*, 425.

[68] R. Lindblad, N. K. Jena, B. Philippe, J. Oscarsson, D. Bi, A. Lindblad, S. Mandal, B. Pal, D. D. Sarma, O. Karis, H. Siegbahn, E. M. J. Johansson, M. Odelius, H. Rensmo, *J. Phys. Chem. C* **2015**, *119*, 1818.

[69] M. Deepa, M. Salado, L. Calio, S. Kazim, S. M. Shivaprasad, S. Ahmad, *Phys. Chem. Chem. Phys.* **2017**, *19*, 4069.

[70] A. Calloni, A. Abate, G. Bussetti, G. Berti, R. Yivlialin, F. Ciccacci, L. Duò, *J. Phys. Chem. C* **2015**, *119*, 21329.

[71] J. You, Z. Hong, Y. M. Yang, Q. Chen, M. Cai, T.-B. Song, C.-C. Chen, S. Lu, Y. Liu, H. Zhou, Y. Yang, *ACS Nano* **2014**, *8*, 1674.

[72] Q. Chen, H. Zhou, Y. Fang, A. Z. Stieg, T.-B. Song, H.-H. Wang, X. Xu, Y. Liu, S. Lu, J. You, P. Sun, J. McKay, M. S. Goorsky, Y. Yang, *Nat. Commun.* **2015**, *6*, 7269.

[73] T. G. Kim, S. W. Seo, H. Kwon, J. Hahn, J. W. Kim, *Phys. Chem. Chem. Phys.* **2015**, *17*, 24342.

[74] F. Liu, C. Ding, Y. Zhang, T. S. Ripolles, T. Kamisaka, T. Toyoda, S. Hayase, T. Minemoto, K. Yoshino, S. Dai, M. Yanagida, H. Noguchi, Q. Shen, *J. Am. Chem. Soc.* **2017**, *139*, 16708.

[75] M. A. Kamarudin, D. Hirotani, Z. Wang, K. Hamada, K. Nishimura, Q. Shen, T. Toyoda, S. Iikubo, T. Minemoto, K. Yoshino, S. Hayase, *J. Phys. Chem. Lett.* **2019**, *10*, 5277.

[76] R. L. Z. Hoye, R. E. Brandt, A. Osherov, V. Stevanović, S. D. Stranks, M. W. B. Wilson, H. Kim, A. J. Akey, J. D. Perkins, R. C. Kurchin, J. R. Poindexter, E. N. Wang, M. G. Bawendi, V. Bulović, T. Buonassisi, *Chem. - A Eur. J.* **2016**, *22*, 2605.

[77] M.-C. Jung, Y. M. Lee, H.-K. Lee, J. Park, S. R. Raga, L. K. Ono, S. Wang, M. R. Leyden, B. D. Yu, S. Hong, Y. Qi, *Appl. Phys. Lett.* **2016**, *108*, 073901.

[78] T. J. Jacobsson, J. P. Correa-Baena, E. Halvani Anaraki, B. Philippe, S. D. Stranks, M. E. F. Bouduban, W. Tress, K. Schenk, J. Teuscher, J. E. Moser, H. Rensmo, A. Hagfeldt, *J. Am. Chem. Soc.* **2016**, *138*, 10331.

[79] S. Bhattacharyya, C. Cardinaud, G. Turban, *J. Appl. Phys.* **1998**, *83*, 4491.

[80] M.-C. Jung, S. Kobori, A. Matsuyama, I. Maeng, Y. M. Lee, H. Kojima, H. Benten, M. Nakamura, *Appl. Phys. Express* **2019**, *12*, 015501.

[81] L. Liu, J. A. McLeod, R. Wang, P. Shen, S. Duhm, *Appl. Phys. Lett.* **2015**, *107*, 061904.

[82] Z. Hawash, S. R. Raga, D.-Y. Son, L. K. Ono, N.-G. Park, Y. Qi, *J. Phys. Chem. Lett.* **2017**, *8*, 3947.

[83] T. L. Barr, S. Seal, *J. Vac. Sci. Technol. A Vacuum, Surfaces, Film.* **1995**, *13*, 1239.

[84] B. P. Payne, M. C. Biesinger, N. S. McIntyre, *J. Electron Spectros. Relat. Phenomena* **2011**, *184*, 29.

[85] S. Neyshtadt, J. P. Jahnke, R. J. Messinger, A. Rawal, T. Segal Peretz, D. Huppert, B. F. Chmelka, G. L. Frey, *J. Am. Chem. Soc.* **2011**, *133*, 10119.

[86] S. Olthof, K. Meerholz, *Sci. Rep.* **2017**, *7*, 40267.

[87] G. Greczynski, L. Hultman, *Prog. Mater. Sci.* **2020**, *107*, 100591.

[88] B. Park, D. U. Lee, D. Jung, W. S. Yang, T. K. Oanh Vu, T. J. Shin, J. Baik, C.-C. Hwang, E. K. Kim, S. Il Seok, *Nano Lett.* **2019**, *19*, 5604.

[89] J. You, Z. Hong, Y. M. Yang, Q. Chen, M. Cai, T.-B. Song, C.-C. Chen, S. Lu, Y. Liu, H. Zhou, Y. Yang, *ACS Nano* **2014**, *8*, 1674.

[90] U. B. Cappel, S. Svanström, V. Lanzilotto, F. O. L. Johansson, K. Aitola, B. Philippe, E. Giangrisostomi, R. Ovsyannikov, T. Leitner, A. Föhlisch, S. Svensson, N. Mårtensson, G. Boschloo, A. Lindblad, H. Rensmo, *ACS Appl. Mater. Interfaces* **2017**, *9*, 34970.

[91] C. S. Fadley, D. A. Shirley, *J. Res. Natl. Bur. Stand. Sect. A Phys. Chem.* **1970**, *74A*, 543.

[92] R. Leckey, in *Surf. Anal. Methods Mater. Sci.* (Ed.: S.R.S.. O'Connor D.J., Sexton B.A.), Springer, Berlin, Heidelberg, **1992**, pp. 291–300.

[93] N. Kitazawa, Y. Watanabe, Y. Nakamura, *J. Mater. Sci.* **2002**, *37*, 3585.

[94] Y. Yamada, T. Nakamura, M. Endo, A. Wakamiya, Y. Kanemitsu, *Appl. Phys. Express* **2014**, *7*, 032302.

[95] Y. Itzhaik, G. Hodes, H. Cohen, *J. Phys. Chem. Lett.* **2011**, *2*, 2872.

[96] A. Givon, H. Piao, J. McMahon, G. Zorn, H. Cohen, *Appl. Phys. Lett.* **2015**, *107*, 173101.

[97] G. Teeter, S. P. Harvey, C. L. Perkins, K. Ramanathan, I. L. Repins, *J. Vac. Sci. Technol. A* **2019**, *37*, 031202.

[98] P. Schulz, E. Edri, S. Kirmayer, G. Hodes, D. Cahen, A. Kahn, *Energy Environ. Sci.* **2014**, *7*, 1377.

[99] S. Wang, T. Sakurai, W. Wen, Y. Qi, *Adv. Mater. Interfaces* **2018**, *5*, 1800260.

[100] Q.-D. Ou, C. Li, Q.-K. Wang, Y.-Q. Li, J.-X. Tang, *Adv. Mater. Interfaces* **2017**, *4*, 1600694.

[101] E. M. Miller, Y. Zhao, C. C. Mercado, S. K. Saha, J. M. Luther, K. Zhu, V. Stevanović, C. L. Perkins, J. Van De Lagemaat, *Phys. Chem. Chem. Phys.* **2014**, *16*, 22122.

[102] J.-P. Yang, M. Meissner, T. Yamaguchi, X.-Y. Zhang, T. Ueba, L.-W. Cheng, S. Ideta, K. Tanaka, X.-H. Zeng, N. Ueno, S. Kera, *Sol. RRL* **2018**, *2*, 1870216.

[103] T. Komesu, X. Huang, T. R. Paudel, Y. B. Losovyj, X. Zhang, E. F. Schwier, Y. Kojima, M. Zheng, H. Iwasawa, K. Shimada, M. I. Saidaminov, D. Shi, A. L. Abdelhady, O. M. Bakr, S. Dong, E. Y. Tsymbal, P. A. Dowben, *J. Phys. Chem. C* **2016**, *120*, 21710.

[104] C. Wang, B. R. Ecker, H. Wei, J. Huang, J.-Q. Meng, Y. Gao, *Phys. Chem. Chem. Phys.* **2017**, *19*, 5361.

[105] D. Niesner, M. Wilhelm, I. Levchuk, A. Osvet, S. Shrestha, M. Batentschuk, C. Brabec, T. Fauster, *Phys. Rev. Lett.* **2016**, *117*, 126401.

[106] F. Zu, P. Amsalem, D. A. Egger, R. Wang, C. M. Wolff, H. Fang, M. A. Loi, D. Neher, L. Kronik, S. Duhm, N. Koch, *J. Phys. Chem. Lett.* **2019**, *10*, 601.

[107] L. E. Polander, P. Pahner, M. Schwarze, M. Saalfrank, C. Koerner, K. Leo, *APL Mater.* **2014**, *2*, 081503.

[108] R. A. Belisle, P. Jain, R. Prasanna, T. Leijtens, M. D. McGehee, *ACS Energy Lett.* **2016**, *1*, 556.

[109] J. Endres, D. A. Egger, M. Kulbak, R. A. Kerner, L. Zhao, S. H. Silver, G. Hodes, B. P. Rand, D. Cahen, L. Kronik, A. Kahn, *J. Phys. Chem. Lett.* **2016**, *7*, 2722.

[110] S. Tao, I. Schmidt, G. Brocks, J. Jiang, I. Tranca, K. Meerholz, S. Olthof, *Nat. Commun.* **2019**, *10*, 2560.

[111] C. Li, J. Wei, M. Sato, H. Koike, Z.-Z. Xie, Y.-Q. Li, K. Kanai, S. Kera, N. Ueno, J.-X. Tang, *ACS Appl. Mater. Interfaces* **2016**, *8*, 11526.

[112] W. A. Dunlap-Shohl, Y. Zhou, N. P. Padture, D. B. Mitzi, *Chem. Rev.* **2019**, *119*, 3193.

[113] J. Burschka, N. Pellet, S. J. Moon, R. Humphry-Baker, P. Gao, M. K. Nazeeruddin, M. Grätzel, *Nature* **2013**, *499*, 316.

[114] Q. Chen, H. Zhou, Z. Hong, S. Luo, H. S. Duan, H. H. Wang, Y. Liu, G. Li, Y. Yang, *J. Am. Chem. Soc.* **2014**, *136*, 622.

[115] F. Fu, L. Kranz, S. Yoon, J. Löckinger, T. Jäger, J. Perrenoud, T. Feurer, C. Gretener, S. Buecheler, A. N. Tiwari, *Phys. Status Solidi Appl. Mater. Sci.* **2015**, *212*, 2708.

[116] W. Nie, H. Tsai, R. Asadpour, J. C. Blancon, A. J. Neukirch, G. Gupta, J. J. Crochet, M. Chhowalla, S. Tretiak, M. A. Alam, H. L. Wang, A. D. Mohite, *Science (80-.).* **2015**, *347*, 522.

[117] N. J. Jeon, J. H. Noh, Y. C. Kim, W. S. Yang, S. Ryu, S. Il Seok, *Nat. Mater.* **2014**, *13*, 897.

[118] L. Gil-Escrig, C. Momblona, M.-G. La-Placa, P. P. Boix, M. Sessolo, H. J. Bolink, *Adv. Energy Mater.* **2018**, *8*, 1703506.

[119] M. Liu, M. B. Johnston, H. J. Snaith, *Nature* **2013**, *501*, 395.

[120] X. Li, D. Bi, C. Yi, J.-D. Décoppet, J. Luo, S. M. Zakeeruddin, A. Hagfeldt, M. Grätzel, *Science (80-.).* **2016**, *353*, 58.

[121] M. M. Lee, J. Teuscher, T. Miyasaka, T. N. Murakami, H. J. Snaith, *Science (80-.).* **2012**, *338*, 643.

[122] J. M. Ball, M. M. Lee, A. Hey, H. J. Snaith, *Energy Environ. Sci.* **2013**, *6*, 1739.

[123] E. J. Juarez-Perez, M. Wußler, F. Fabregat-Santiago, K. Lakus-Wollny, E. Mankel, T. Mayer, W. Jaegermann, I. Mora-Sero, *J. Phys. Chem. Lett.* **2014**, *5*, 680.

[124] J. P. Correa Baena, L. Steier, W. Tress, M. Saliba, S. Neutzner, T. Matsui, F. Giordano, T. J. Jacobsson, A. R. Srimath Kandada, S. M. Zakeeruddin, A. Petrozza, A. Abate, M. K. Nazeeruddin, M. Grätzel, A. Hagfeldt, *Energy Environ. Sci.* **2015**, *8*, 2928.

[125] K.-C. Wang, J.-Y. Jeng, P.-S. Shen, Y.-C. Chang, E. W.-G. Diau, C.-H. Tsai, T.-Y. Chao, H.-C. Hsu, P.-Y. Lin, P. Chen, T.-F. Guo, T.-C. Wen, *Sci. Rep.* **2015**, *4*, 4756.

[126] P. Docampo, J. M. Ball, M. Darwich, G. E. Eperon, H. J. Snaith, *Nat. Commun.* **2013**, *4*, 2761.

[127] H. Tian, B. Xu, H. Chen, E. M. J. Johansson, G. Boschloo, *ChemSusChem* **2014**, *7*, 2150.

[128] J. M. Azpiroz, E. Mosconi, J. Bisquert, F. De Angelis, *Energy Environ. Sci.* **2015**, *8*, 2118.

[129] J. H. Kim, P. W. Liang, S. T. Williams, N. Cho, C. C. Chueh, M. S. Glaz, D. S. Ginger, A. K. Y. Jen, *Adv. Mater.* **2015**, *27*, 695.

[130] T. Liu, K. Chen, Q. Hu, R. Zhu, Q. Gong, *Adv. Energy Mater.* **2016**, *6*, 1600457.

[131] J. C. Yu, J. A. Hong, E. D. Jung, D. Bin Kim, S.-M. Baek, S. Lee, S. Cho, S. S. Park, K. J. Choi, M. H. Song, *Sci. Rep.* **2018**, *8*, 1070.

[132] X. Liu, C. Wang, L. Lyu, C. Wang, Z. Xiao, C. Bi, J. Huang, Y. Gao, *Phys. Chem. Chem. Phys.* **2015**, *17*, 896.

[133] M.-F. Lo, Z.-Q. Guan, T.-W. Ng, C.-Y. Chan, C.-S. Lee, *Adv. Funct. Mater.* **2015**, *25*, 1213.

[134] S. Chen, T. W. Goh, D. Sabba, J. Chua, N. Mathews, C. H. A. Huan, T. C. Sum, *APL Mater.* **2014**, *2*, 081512.

[135] C. Wang, Y. Li, X. Xu, C. Wang, F. Xie, Y. Gao, *Chem. Phys. Lett.* **2016**, *649*, 151.

[136] Y. Ogomi, A. Morita, S. Tsukamoto, T. Saitho, N. Fujikawa, Q. Shen, T. Toyoda, K. Yoshino, S. S. Pandey, T. Ma, S. Hayase, *J. Phys. Chem. Lett.* **2014**, *5*, 1004.

[137] Q. Wang, Y. Shao, H. Xie, L. Lyu, X. Liu, Y. Gao, J. Huang, *Appl. Phys. Lett.* **2014**, *105*, 163508.

[138] R. Wang, M.-P. Zhuo, J. Li, T. Zhai, J. Yang, K. Fu, L.-S. Liao, L. Liu, S. Duhm, *Adv. Mater. Interfaces* **2019**, *6*, 1801827.

[139] J. Emara, T. Schnier, N. Pourdavoud, T. Riedl, K. Meerholz, S. Olthof, *Adv. Mater.* **2016**, *28*, 553.

[140] Q. Sun, P. Fassl, Y. Vaynzof, *ACS Appl. Energy Mater.* **2018**, *1*, 2410.

[141] N. Ahn, D.-Y. Son, I.-H. Jang, S. M. Kang, M. Choi, N.-G. Park, *J. Am. Chem. Soc.* **2015**, *137*, 8696.

[142] W. Zhang, M. Saliba, D. T. Moore, S. K. Pathak, M. T. Hörantner, T. Stergiopoulos, S. D. Stranks, G. E. Eperon, J. A. Alexander-Webber, A. Abate, A. Sadhanala, S. Yao, Y. Chen, R. H. Friend, L. A. Estroff, U. Wiesner, H. J. Snaith, *Nat. Commun.* **2015**, *6*, 6142.

[143] D. J. Morgan, *J. Electron Spectros. Relat. Phenomena* **2019**, *231*, 109.

[144] H. Piao, N. Fairley, J. Walton, *Surf. Interface Anal.* **2013**, *45*, 1742.

[145] F. Zu, C. M. Wolff, M. Ralaiarisoa, P. Amsalem, D. Neher, N. Koch, *ACS Appl. Mater. Interfaces* **2019**, *11*, 21578.

[146] C. Das, M. Wussler, T. Hellmann, T. Mayer, W. Jaegermann, *Phys. Chem. Chem. Phys.* **2018**, *20*, 17180.

[147] F.-S. Zu, P. Amsalem, I. Salzmann, R.-B. Wang, M. Ralaiarisoa, S. Kowarik, S. Duhm, N. Koch, *Adv. Opt. Mater.* **2017**, *5*, 1700139.

[148] Q. Sun, P. Fassl, D. Becker-Koch, A. Bausch, B. Rivkin, S. Bai, P. E. Hopkinson, H. J.

Snaith, Y. Vaynzof, *Adv. Energy Mater.* **2017**, *7*, 1700977.

[149] X. Tang, M. Brandl, B. May, I. Levchuk, Y. Hou, M. Richter, H. Chen, S. Chen, S. Kahmann, A. Osvet, F. Maier, H. P. Steinrück, R. Hock, G. J. Matt, C. J. Brabec, *J. Mater. Chem. A* **2016**, *4*, 15896.

[150] J. F. Verwey, *J. Phys. Chem. Solids* **1970**, *31*, 163.

[151] R. A. Kerner, T. H. Schloemer, P. Schulz, J. J. Berry, J. Schwartz, A. Sellinger, B. P. Rand, *J. Mater. Chem. C* **2019**, *7*, 5251.

[152] R. A. Kerner, T. H. Schloemer, P. Schulz, J. J. Berry, J. Schwartz, A. Sellinger, B. P. Rand, *J. Mater. Chem. C* **2019**, *7*, 5244.

[153] A. Alberti, I. Deretzis, G. Pellegrino, C. Bongiorno, E. Smecca, G. Mannino, F. Giannazzo, G. G. Condorelli, N. Sakai, T. Miyasaka, C. Spinella, A. La Magna, *ChemPhysChem* **2015**, *16*, 3064.

[154] R. P. Xu, Y. Q. Li, T. Y. Jin, Y. Q. Liu, Q. Y. Bao, C. O'Carroll, J. X. Tang, *ACS Appl. Mater. Interfaces* **2018**, *10*, 6737.

[155] C. C. Boyd, R. Cheacharoen, T. Leijtens, M. D. McGehee, *Chem. Rev.* **2019**, *119*, 3418.

[156] S. Chen, X. Du, D. Lin, F. Xie, W. Xie, L. Gong, W. Zhang, P. Liu, J. Chen, *J. Electron Spectros. Relat. Phenomena* **2018**, *229*, 108.

[157] N.-K. Kim, Y. H. Min, S. Noh, E. Cho, G. Jeong, M. Joo, S.-W. Ahn, J. S. Lee, S. Kim, K. Ihm, H. Ahn, Y. Kang, H.-S. Lee, D. Kim, *Sci. Rep.* **2017**, *7*, 4645.

[158] B. J. Foley, D. L. Marlowe, K. Sun, W. A. Saidi, L. Scudiero, M. C. Gupta, J. J. Choi, *Appl. Phys. Lett.* **2015**, *106*, 243904.

[159] K. Domanski, J. P. Correa-Baena, N. Mine, M. K. Nazeeruddin, A. Abate, M. Saliba, W. Tress, A. Hagfeldt, M. Grätzel, *ACS Nano* **2016**, *10*, 6306.

[160] L. Etgar, P. Gao, Z. Xue, Q. Peng, A. K. Chandiran, B. Liu, M. K. Nazeeruddin, M.

Grätzel, *J. Am. Chem. Soc.* **2012**, *134*, 17396.

[161] W. A. Laban, L. Etgar, *Energy Environ. Sci.* **2013**, *6*, 3249.

[162] L. Zhao, R. A. Kerner, Z. Xiao, Y. L. Lin, K. M. Lee, J. Schwartz, B. P. Rand, *ACS Energy Lett.* **2016**, *1*, 595.

[163] F. J. Ramos, T. Maindron, S. Béchu, A. Rebai, M. Frégnaux, M. Bouttemy, J. Rousset, P. Schulz, N. Schneider, *Sustain. Energy Fuels* **2018**, *2*, 2468.

[164] Y. Yuan, J. Huang, *Acc. Chem. Res.* **2016**, *49*, 286.

[165] S. van Reenen, M. Kemerink, H. J. Snaith, *J. Phys. Chem. Lett.* **2015**, *6*, 3808.

[166] P. Calado, A. M. Telford, D. Bryant, X. Li, J. Nelson, B. C. O'Regan, P. R. F. Barnes, *Nat. Commun.* **2016**, *7*, 13831.

[167] Z. Li, C. Xiao, Y. Yang, S. P. Harvey, D. H. Kim, J. A. Christians, M. Yang, P. Schulz, S. U. Nanayakkara, C.-S. Jiang, J. M. Luther, J. J. Berry, M. C. Beard, M. M. Al-Jassim, K. Zhu, *Energy Environ. Sci.* **2017**, *10*, 1234.

[168] K. Domanski, B. Roose, T. Matsui, M. Saliba, S.-H. Turren-Cruz, J.-P. Correa-Baena, C. R. Carmona, G. Richardson, J. M. Foster, F. De Angelis, J. M. Ball, A. Petrozza, N. Mine, M. K. Nazeeruddin, W. Tress, M. Grätzel, U. Steiner, A. Hagfeldt, A. Abate, *Energy Environ. Sci.* **2017**, *10*, 604.

[169] S. P. Harvey, F. Zhang, A. Palmstrom, J. M. Luther, K. Zhu, J. J. Berry, *ACS Appl. Mater. Interfaces* **2019**, *11*, 30911.

[170] Y. Busby, A. Agresti, S. Pescetelli, A. Di Carlo, C. Noel, J.-J. Pireaux, L. Houssiau, *Mater. Today Energy* **2018**, *9*, 1.

[171] S. Heo, G. Seo, Y. Lee, M. Seol, S. H. Kim, D.-J. Yun, Y. Kim, K. Kim, J. Lee, J. Lee, W. S. Jeon, J. K. Shin, J. Park, D. Lee, M. K. Nazeeruddin, *Adv. Mater.* **2019**, *31*, 1805438.

[172] Y. Zhou, F. Wang, H.-H. Fang, M. A. Loi, F.-Y. Xie, N. Zhao, C.-P. Wong, *J. Mater.*

Chem. A **2016**, *4*, 16191.

[173] C. Noël, S. Pescetelli, A. Agresti, A. Franquet, V. Spampinato, A. Felten, A. di Carlo, L. Houssiau, Y. Busby, *Materials (Basel).* **2019**, *12*, 726.

[174] B. Philippe, M. Saliba, J.-P. Correa-Baena, U. B. Cappel, S.-H. Turren-Cruz, M. Grätzel, A. Hagfeldt, H. Rensmo, *Chem. Mater.* **2017**, *29*, 3589.

[175] B. Conings, L. Baeten, C. De Dobbelaere, J. D'Haen, J. Manca, H. G. Boyen, *Adv. Mater.* **2014**, *26*, 2041.

[176] S. R. Raga, M. C. Jung, M. V. Lee, M. R. Leyden, Y. Kato, Y. Qi, *Chem. Mater.* **2015**, *27*, 1597.

[177] W. Huang, J. S. Manser, P. V. Kamat, S. Ptasinska, *Chem. Mater.* **2016**, *28*, 303.

[178] I. A. Shkrob, T. W. Marin, *J. Phys. Chem. Lett.* **2014**, *5*, 1066.

[179] J. D. McGettrick, K. Hooper, A. Pockett, J. Baker, J. Troughton, M. Carnie, T. Watson, *Mater. Lett.* **2019**, *251*, 98.

[180] R. A. Kerner, P. Schulz, J. A. Christians, S. P. Dunfield, B. Dou, L. Zhao, G. Teeter, J. J. Berry, B. P. Rand, *APL Mater.* **2019**, *7*, 041103.

[181] P. Faßl, Exploration of Properties, Stability and Reproducibility of Perovskite Solar Cells, Ruperto-Carola University of Heidelberg, **2018**.

[182] M. Ralaiarisoa, I. Salzmann, F. Zu, N. Koch, *Adv. Electron. Mater.* **2018**, *4*, 1800307.

[183] M. Ralaiarisoa, Y. Rodríguez, I. Salzmann, L. Vaillant, N. Koch, *Appl. Phys. A* **2019**, *125*, 470.

[184] A. M. A. Leguy, Y. Hu, M. Campoy-Quiles, M. I. Alonso, O. J. Weber, P. Azarhoosh, M. van Schilfgaarde, M. T. Weller, T. Bein, J. Nelson, P. Docampo, P. R. F. Barnes, *Chem. Mater.* **2015**, *27*, 3397.

[185] H.-H. Fang, S. Adjokatse, H. Wei, J. Yang, G. R. Blake, J. Huang, J. Even, M. A. Loi, *Sci. Adv.* **2016**, *2*, e1600534.

[186] G. N. Hall, M. Stuckelberger, T. Nietzold, J. Hartman, J.-S. Park, J. Werner, B. Niesen, M. L. Cummings, V. Rose, C. Ballif, M. K. Chan, D. P. Fenning, M. I. Bertoni, *J. Phys. Chem. C* **2017**, *121*, 25659.

[187] Y. Li, X. Xu, C. Wang, C. Wang, F. Xie, J. Yang, Y. Gao, *J. Phys. Chem. C* **2015**, *119*, 23996.

[188] M. Anaya, J. F. Galisteo-López, M. E. Calvo, J. P. Espinós, H. Míguez, *J. Phys. Chem. Lett.* **2018**, *9*, 3891.

[189] N. Aristidou, C. Eames, I. Sanchez-Molina, X. Bu, J. Kosco, M. S. Islam, S. A. Haque, *Nat. Commun.* **2017**, *8*, 15218.

[190] E. A. Kraut, R. W. Grant, J. R. Waldrop, S. P. Kowalczyk, *Phys. Rev. B* **1983**, *28*, 1965.

[191] I. G. Hill, A. Rajagopal, A. Kahn, *J. Appl. Phys.* **1998**, *84*, 3236.

[192] E. M. Miller, D. M. Kroupa, J. Zhang, P. Schulz, A. R. Marshall, A. Kahn, S. Lany, J. M. Luther, M. C. Beard, C. L. Perkins, J. van de Lagemaat, *ACS Nano* **2016**, *10*, 3302.

[193] T. Sueyoshi, H. Fukagawa, M. Ono, S. Kera, N. Ueno, *Appl. Phys. Lett.* **2009**, *95*, 183303.

[194] H. Kawai, G. Giorgi, A. Marini, K. Yamashita, *Nano Lett.* **2015**, *15*, 3103.

[195] M.-I. Lee, A. Barragán, M. N. Nair, V. L. R. Jacques, D. Le Bolloc'h, P. Fertey, K. Jemli, F. Lédée, G. Trippé-Allard, E. Deleporte, A. Taleb-Ibrahimi, A. Tejeda, *J. Phys. D. Appl. Phys.* **2017**, *50*, 26LT02.

[196] F. Zu, P. Amsalem, M. Ralaiarisoa, T. Schultz, R. Schlesinger, N. Koch, *ACS Appl. Mater. Interfaces* **2017**, *9*, 41546.

[197] T. Gallet, D. Grabowski, T. Kirchartz, A. Redinger, *Nanoscale* **2019**, *11*, 16828.

Table of Contents

Keywords Halide Perovskites, Photoemission Spectroscopy, Electronic Properties, Energy Materials Solar Cells

Solène Béchu*, Maryline Ralaiarisoa, Arnaud Etcheberry and Philip Schulz*

Photoemission Spectroscopy Characterization of Halide Perovskites

ToC figure 55 mm broad × 50 mm high

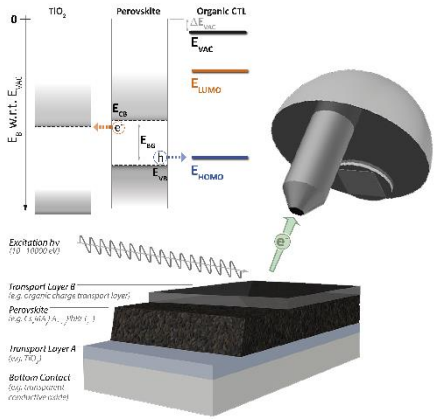

ToC text:

The central focus of this review is on the possibilities and intricacies in the use of photoemission spectroscopy (PES) techniques for research on halide perovskite materials. Accurate description of the chemical and electronical properties can thus be obtained, by coupling complementary PES techniques, such as ultraviolet photoemission spectroscopy, inverse photoemission spectroscopy and X-ray photoemission spectroscopy.